HHS Public Access

Author manuscript

Life Sci. Author manuscript; available in PMC 2025 June 15.

Published in final edited form as:

Life Sci. 2025 June 15; 371: 123559. doi:10.1016/j.lfs.2025.123559.

Type I interferon protects against bone loss in periodontitis by mitigating an interleukin (IL)-17-neutrophil axis

Jinmei Zhang[a,b], **Qiong Ding**[a,b], **Angela X. Wang**[a,b], **Maoxuan Lin**[c], **Ning Yu**[d], **Kevin Moss**[e], **Megumi A. Williamson**[f], **Di Miao**[a,b], **Julie T. Marchesan**[g], **Erliang Zeng**[h], **Wei Shi**[h], **Hongli Sun**[a,i], **Yu Leo Lei**[j], **Shaoping Zhang**[a,b,*]

[a]Iowa Institute of Oral Health Research, University of Iowa College of Dentistry, Iowa City, IA, USA

[b]Periodontics Department, University of Iowa College of Dentistry, Iowa City, IA, USA

[c]Department of Neurology, Brigham and Women's Hospital, Harvard Medical School, Boston, MA, USA

[d]The Forsyth Institute, Cambridge, MA, USA

[e]Department of Biostatistics and Health Data Science, School of Medicine, University of Indiana, Indianapolis, IN, USA

[f]Department of Surgical Sciences, School of Dental Medicine, East Carolina University, Greenville, NC, USA

[g]Division of Comprehensive Oral Health, Periodontology, Adams School of Dentistry, University of North Carolina at Chapel Hill, Chapel Hill, NC, USA

[h]Division of Biostatistics and Computational Biology, University of Iowa College of Dentistry, Iowa City, IA, USA

[i]Department of Oral and Maxillofacial Surgery, University of Iowa College of Dentistry, Iowa City, IA, USA

*Corresponding author at: Iowa Institute of Oral Health Research, Periodontics Department, University of Iowa College of Dentistry, Room 412 Dental Science Building, 801 Newton Road, Iowa City, IA 52242, USA. shaoping-zhang@uiowa.edu (S. Zhang).

CRediT authorship contribution statement

Jinmei Zhang: Writing – review & editing, Writing – original draft, Visualization, Validation, Investigation, Formal analysis, Data curation. **Qiong Ding:** Writing – review & editing, Data curation. **Angela X. Wang:** Writing – review & editing, Validation, Investigation, Formal analysis. **Maoxuan Lin:** Writing – review & editing, Visualization, Software, Formal analysis, Data curation. **Ning Yu:** Writing – review & editing, Resources, Investigation. **Kevin Moss:** Writing – review & editing, Software, Formal analysis. **Megumi A. Williamson:** Writing – review & editing, Resources. **Di Miao:** Writing – review & editing, Validation, Investigation. **Julie T. Marchesan:** Writing – review & editing, Funding acquisition, Formal analysis, Conceptualization. **Erliang Zeng:** Writing – review & editing, Visualization, Software, Formal analysis. **Wei Shi:** Writing – review & editing, Visualization, Software, Formal analysis. **Hongli Sun:** Writing – review & editing, Resources, Methodology. **Yu Leo Lei:** Writing – review & editing, Resources, Methodology, Funding acquisition, Conceptualization. **Shaoping Zhang:** Writing – review & editing, Writing – original draft, Visualization, Project administration, Methodology, Funding acquisition, Formal analysis, Data curation, Conceptualization.

Declaration of competing interest

The authors declare no conflict of interest.

Appendix A. Supplementary data

Supplementary data to this article can be found online at https://doi.org/10.1016/j.lfs.2025.123559.

[j]Departments of Head and Neck Surgery, Cancer Biology, and Translational Molecular Pathology, University of Texas M.D. Anderson Cancer Center, Houston, TX, USA

Abstract

Type I interferons (IFNs-I), a group of pleiotropic cytokines, critically modulate host response in various inflammatory diseases. However, the role of the IFN-I pathway in periodontitis remains largely unknown. In this report, we describe that the IFN-β levels in the gingival crevicular fluid of human subjects were negatively associated with periodontitis and clinical gingival inflammation. Disruption of IFN-I signaling worsened alveolar bone resorption in a ligature-induced periodontitis murine model. Deficiency of the IFN-I pathway resulted in an exaggerated inflammatory response in myeloid cells and drastically increased the interleukin-17 (IL-17)-mediated neutrophil recruitment in the gingiva. We further identified that the myeloid lineage-specific IFN-I response was essential in safeguarding against periodontal inflammation by suppressing the IL-17-producing γδ T cells in gingiva. IFN-I signaling also directly repressed osteoclastogenesis in monocytes, which are precursor cells for osteoclasts. Therefore, our findings demonstrate that an integral myeloid-specific IFN-I pathway protects against bone loss by keeping the IL-17-neutrophil axis in check and directly inhibiting osteoclast formation in periodontitis.

Keywords

Type-I interferon (IFN-I); Periodontitis; Neutrophil; Interleukin-17 (IL-17); Osteoclastogenesis; Monocytes; Single-cell analysis

1. Introduction

Periodontitis is an irreversible inflammatory disease initiated by plaque dysbiosis. If not appropriately managed, this extremely prevalent oral disease will lead to the irreversible breakdown of the periodontal supporting apparatus and, eventually, tooth loss [1–4]. This common inflammatory disease in the oral cavity is also closely associated with various systemic diseases [3,5,6]. The core mechanism of tissue damage to the periodontal ligament attachment and alveolar bone affected by periodontal disease is the dysregulation of the inflammatory response [7,8]. Our previous studies have shown that overactivation of the cytokine interleukin-17 (IL-17), in the absence of IL-10 and IL-1 receptor antagonist (IL-RA), led to periodontal tissue destruction [9–11].

Type I interferon (IFN-I) molecules are a family of pleiotropic cytokines produced by various types of cells [11–13]. The intracellular signaling of IFN-α/-−β, which are classical IFN-I family members, requires the binding of the cytokine ligand to a heterodimeric transmembrane receptor, the IFN-α receptor (IFNAR), which is composed of the IFNAR1 and the IFNAR2 subunits. The IFNAR is widely expressed by different cells [11,12]. The biological activity of IFNs-I is profoundly involved in various infectious and inflammatory diseases. The anti-viral response of IFNs-I is well-known and has been studied extensively [13,14]. However, the role of IFN-α/− β in inflammation appears to be more complex. IFN-I is frequently involved in the pathogenicity of systemic lupus erythematosus by its ability to promote the differentiation of monocytes into dendritic cells with enhanced antigen-

presenting capacities or to induce plasma cell differentiation [15–17]. However, IFN-I has a beneficial effect on multiple sclerosis (MS), a neurological degenerative autoimmune disorder. IFN-β1a is used clinically to treat certain stages of MS. The conditional deletion of *Ifnar1* in mouse monocytes and macrophages or dendritic cells exacerbated the disease activity of the experimental autoimmune encephalomyelitis (EAE), an animal model that recapitulates many characteristics of MS [18,19]. Additionally, the suppression of EAE by IFN-β can be achieved by suppressing the T-helper 17 (Th17) cell expansion [20].

Other than immunoregulation, IFN-β has a potent inhibitory effect on osteoclastogenesis. *Ifnar1*$^{-/-}$ mice exhibited severe osteopenia due to increased osteoclasts [21]. Such a direct role in bone homeostasis was mediated by interfering with the expression of c-Fos, an essential transcriptional factor for osteoclast differentiation [21]. Other groups have reported that upstream signals or inducers for IFN-I activation, such as cyclic dinucleotides and the immune signaling adaptor stimulator of interferon genes (STING), drastically inhibited osteoclast differentiation [22,23].

The effect of IFN-I on periodontal disease remains elusive. In a case-control study, Acar et al. reported that the gingival crevicular fluid (GCF) level of IFN-α in patients with severe congenital neutropenia was significantly less than the level of healthy controls who also had better periodontal status and less gingival inflammation than the neutropenic patients [24]. Conversely, another group showed that the transcriptional level of *IFNA* was significantly higher in tissues with periodontitis than in biopsies without periodontitis [25]. Using a blocking antibody to IFNAR1, Mizraji et al. concluded that the IFN-I upregulation by infection of *Porphyromonas gingivalis* (*P. gingivalis*), a well-studied periodontal disease-associated bacterium, disrupted the innate immune response in gingiva and was associated with a constitutively primed T cell response, which exacerbated periodontal bone loss [26]. However, orally administered IFN-α4 effectively inhibited naturally occurring gingivitis in dogs [27]. The topical treatment of IFN-α in dogs also reduced the detection of different sub-strains of *Porphyromonas gulae*, a major periodontal pathogen in dogs, and improved periodontal status [28].

In this report, using clinical data and a ligature-induced murine periodontitis (LIP) model, we aimed to assess the role of the IFN-I pathway in periodontal disease. We further focused on the effect of the IFN-I signaling on myeloid monocytic cells in periodontitis. Overall, we found that the IFN-I pathway protects against periodontitis bone loss by dampening an IL-17-neutrophil axis and directly inhibiting osteoclastogenesis. The integrity of the IFN-I pathway in monocytic cells is indispensable in converging such dual defensive mechanisms in thwarting periodontal bone loss.

2. Materials and methods

2.1. Human subjects and biological sample collection

A total of 374 subjects enrolled in the dental Atherosclerosis Risk in Communities (ARIC) cohort were included in this study. All subjects provided informed written consent to an approved institutional review board (IRB) on research in which human subjects are involved at UNC-CH (No.96–090) and each ARIC examination center. The ARIC study was

originally designed to measure the associations of established and suspected coronary heart disease risk factors with atherosclerosis and the incidence of coronary heart disease from four U.S. communities [29]. Those 374 participants were all self-reported non-smokers and non-diabetic and were not taking any medications, such as statins, for reducing cholesterol levels. They all had a complete periodontal examination record, which includes probing depth (PD), attachment level (AL), bleeding on probing (BOP) and gingival index by Löe & Silness criteria [30]. Detailed information for periodontal examination and clinical indices of the ARIC participants was described previously [31,32]. Gingival crevicular fluid was collected using Harco PerioPaper strip (Tustin, CA, USA) from the mesiobuccal site of each first molar or, if missing, an alternate site for ARIC participants as previously described [33]. The volume of GCF samples was determined by a Periotron (Oral Flow, Inc. New York, NY, USA) for the calculation of the concentration of cytokines assed by multiplex as described below. Those GCF strips were then immediately flash-frozen at chairside and stored in liquid nitrogen at the University of North Carolina at Chapel Hill (UNC-CH) Adams School of Dentistry until use. The archived GCF samples were retrieved for all 374 participants for multiplex proteomics analysis, as described below [9].

Gingival biopsies were collected for immunohistochemistry staining from a periodontitis-free participant who received a clinical crown lengthening procedure and a periodontitis patient during a periodontal resective surgery. The biopsied site from the periodontitis patient manifested clinical attachment loss (CAL = 5 mm) and deep probing depth (PD = 6 mm). Subjects provided informed consent to an approved IRB research protocol at the University of Iowa College of Dentistry.

2.2. Mice

IFNbeta1/enhanced yellow fluorescent protein (EYFP) reporter mice (*Ifnb*^{mob}, strain #010818) [34], wild-type (WT) C57BL/6 J mice (strain #000664), *Ifnar1*$^{fl/fl}$ (strain #028256), *LysMcre* mice (strain #004781) were all purchased from Jackson Laboratory. IFNAR1-deficient (*Ifnar1*$^{-/-}$) C57BL/6 mice were generous gifts from Dr. Yu Leo Lei at the University of Michigan School of Dentistry. *Act1*$^{-/-}$ (*Traf3ip2*$^{-/-}$) C57BL/6 mice were generous gifts from Dr. Ulrich Siebenlist at the National Institute of Allergy and Infectious Diseases. *Act1*$^{-/-}$ mice were bred with *Ifnar1*$^{-/-}$ mice to generate the *Ifnar1*$^{-/-}$*Act1*$^{-/-}$ double knockout mouse strain. *Ifnar1*$^{fl/fl}$ mice were crossed wtih *LysMcre* mice to generate myeloid IFNAR1-deficient mice *LysMcre*-*Ifnar1*$^{fl/fl}$ and littermate controls *Ifnar1*$^{fl/fl}$. All animals used in the ligature-induced periodontitis model were between 10- and 12-week-old. We used gender- and age-matched mice in animal studies. Mice were housed and handled in a specific pathogen-free vivarium (Animal Biosafety Level 1). All components of animal studies were approved by the Institutional Animal Care and Use Committee (IACUC) at the University of Iowa (No.1082174).

2.3. Ligature-induced periodontitis (LIP) model

The ligature-induced periodontitis bone loss model that was described previously was performed in mice [35]. For most experiments, mice were euthanized by CO_2 on day 10 after ligature placement. Mice maxillae were fixed with 4 % paraformaldehyde for micro-computed tomography (μCT) and histology analyses.

2.4. Neutrophil depletion

Neutrophils were depleted in *Ifnar1*$^{-/-}$ mice according to a previous protocol with minor modification [4]. Briefly, 100 mg of a rat anti-mouse Ly6G antibody (1A8, catalog # BE0075–1, BioXCell, NH, USA) in 150 μl dilution buffer (catalog # IP0070, BioXCell) was administrated intraperitoneally (IP) in *Ifnar1*$^{-/-}$ mice one day before (day − 1) and repeated on day 3 after ligature placement. Mice treated with 100 μg rat IgG2a isotype antibody (2A3, catalog # BP0089, BioXCell) served as controls. On day 6, gingival and blood samples were harvested for flow cytometry to confirm the neutrophil depletion efficiency.

2.5. Alveolar bone loss measurement

The mouse maxillae described above were sent to the Small Animal Imaging Core Facility at the University of Iowa for micro-CT (μCT) scanning. The scanning images were acquired and processed by Zeiss Xradia 520 Versa. The distance between the cementoenamel junction (CEJ) to the alveolar bone crest (ABC), which reflects the linear periodontal alveolar bone loss, was measured at the buccal side of the first molar (Mo1) distal root, the buccal side of the second molar (Mo2) mesial root, and the palatal root of both molars. The measurement was accomplished using MicroView software (Parallax Innovations, Ilderton, Canada). Using anatomical tooth landmarks, we standardized the alveolar bone loss measurement across samples by aligning maxillary samples in horizontal, sagittal, and coronal planes [4,35]. In addition, bone volume fraction (Bone volume/ total volume or BV/TV) was measured and calculated from the region of interest (ROI) for each sample by Dragonfly software (Comet Technologies Canada Inc., Montreal, Canada).

2.6. Immunohistochemistry (IHC) and Immunofluorescence (IF)

The human gingival biopsy samples were fixed overnight with paraformaldehyde, then paraffin-embedded and sectioned into 5 μm slides. The slides were heated to activate antigen retrieval. Then, the slides were stained with a rabbit polyclonal primary antibody anti-IFN-β (catalog # BNP1–77288, Novus Biologicals, Centennial, CO, USA) at a dilution of 1:400. A biotinylated anti-rabbit IgG secondary antibody (catalog # CTS005, R&D Systems, Minneapolis, MN, USA) was used according to the manufacturer's instructions.

Mouse maxillary specimens were decalcified by freshly made 10 % EDTA (pH = 7.4) solution every two days for 10 days. After embedding, tissue specimens were sectioned into 5 μm slides. Heat-induced antigen epitope retrieval was achieved with an acidic solution (catalog # CTS014, R&D Systems). After incubation with the primary antibody, either a rat anti-Ly6g/Gr1 antibody (catalog # LS-C112469, LifeSpan BioSciences, Lynnwood, WA, USA) with a dilution of 1:200 or a rabbit anti-IL-17 (catalog # ab79056, Abcam, Waltham, MA, USA) with a dilution of 1:200 at 4 °C overnight, the slides were washed and incubated with an anti-rat IgG secondary antibody included in an ImmPRESS HRP Goat Anti-Rat IgG Kit (catalog # MP-7444, Vector Laboratories, Newark, CA, USA) or an anti-rabbit IgG secondary antibody included in a Vectastain Elite ABC-HRP kit (catalog # PK-6101, Vector Laboratories), respectively. DAB (3,3'-Diainobenzidine) was used as the chromogen for staining. Nuclei were counterstained with hematoxylin. IHC images were captured by a Nikon bright-field microscope (Eclipse Ts2, Nikon, Japan).

For IF staining, a primary rabbit anti-GFP antibody (catalog # 225314, Abcam) was used to react against EYFP of the reporter mice. After washing, tissue sections were incubated with an anti-rabbit IgG antibody Alexa fluor 488 (catalog # A-11070, Invitrogen, Waltham, MA, USA). After staining, mouse maxillary tissue sections were mounted with an antifade DAPI-containing mounting medium (catalog # H-2000, Vector Laboratories) and observed under an LSM 710 confocal laser scanning microscope (Zeiss, Germany).

2.7. Tartrate-resistant acid phosphatase (TRAP) staining

Mouse maxillary tissue sections were prepared, as described above. A tartrate-resistant acid phosphatase (TRAP) kit (catalog # 387 A-1KT, Sigma-Aldrich, St. Louis, MO, USA) was used to stain osteoclasts according to the manufacturer's instructions. TRAP-positive ($TRAP^+$) multinucleated cells were counted under a bright-field microscope. The $TRAP^+$ osteoclasts were counted in three sections for each mouse maxillary sample. Osteoclasts were defined as TRAP+ with more than three nuclei in the *ex vivo* differentiated osteoclast cell culture.

2.8. Bone marrow-derived monocytic cell isolation, differentiation, and treatment

Bone marrow-derived monocytic cells (BMDMs) were isolated from tibias and femurs of the six-week-old C57BL/6 WT and *Ifnar1*$^{-/-}$ mice. Briefly, tibias and femurs were collected from mice under sterile conditions. Both ends of bones were cut with scissors, and the bone marrows were flushed out with cold PBS using a 20-gauge needle. After filtering and centrifugation, bone marrow cells were cultured in a-MEM supplemented with 10 % FBS and 1 % penicillin/streptomycin. After 3 h of culturing, non-adherent cells were removed from the culture. The adherent BMDMs were then cultured in a 48-well plate with a seeding density of 5×10^5 cells per well in the presence of 30 ng/ml macrophage colony-stimulating factor (M-CSF, catalog # 416-ML-010/*CF*, R&D Systems) in the culture medium to allow differentiation into primary macrophages. After three days of differentiation, those differentiated macrophages were stimulated with *E. coli* LPS (catalog # L4391, Sigma-Aldrich) at a concentration of 100 ng/ml in the absence or presence of recombinant murine IFN-β (catalog # 8234-MB-010/*CF*, R&D Systems) at a concentration of 1 ng/ml for 18 h.

For osteoclast differentiation, the BMDMs were cultured with 30 ng/ml M-CSF for 3 days, and then, 10 ng/ml RANKL (catalog # 462-TEC-010/*CF*, R&D Systems) was added to the culture for an additional 5 days. Those cells were co-treated in the absence or presence of murine IFN-β with a concentration of either 3 ng/ml or 0.3 ng/ml.

2.9. Co-culture of naïve CD4+ T cells and BMDM-derived macrophages

The *ex vivo* co-culture model was created based on previously published methods with modifications [19,36]. Single-cell suspensions were prepared from the spleen of the WT mice. Then, naïve CD4+ T cells were enriched from spleen cells by a MidiMACS separator (catalog # 130–042–302, Miltenyi Biotec, Germany) and an LS column (catalog # 130–042–401, Miltenyi Biotec) with a mouse $CD4^+$ T cell isolation kit (catalog # 130–104–454, Miltenyi Biotec) following the manufacturer's protocol. Isolated CD4+ T cells were cultured in X-VIVO medium (catalog # 04–418Q, Lonza, Switzerland) stimulated with 1

μg/ml anti-CD3 antibody that was coated in U-bottom 96-well plates (catalog # 55058, BD Biosciences, Franklin Lakes, NJ, USA). Cells were collected after 16 h stimulation. BMDMs were isolated from WT or *Ifnar1*$^{-/-}$ mice and differentiated into macrophages, as mentioned above. 1 × 10^6 *ex vivo* differentiated macrophages were seeded in a 12-well plate and challenged with 100 ng/ml *E. coli* LPS 20 h before co-culture. 5 × 10^6 stimulated $CD4^+$ T cells were transferred to each well of the differentiated macrophages at a ratio of 5:1 and then stimulated with 1 μg/ml anti-CD28 antibody (catalog # 553295,BD Biosciences). Supernatants and cells were analyzed on day 3 post-coculture for ELISA and flow cytometry, respectively.

2.10. Workflow of single-cell RNA-sequencing (scRNA-seq)

To prepare single-cell suspensions, gingival tissues were collected from mice used in the LIP model, minced, and incubated with RPMI 1640 medium containing 0.15 mg/ml DNase (catalog # DN25–100MG, Sigma-Aldrich) and 3.2 mg/ml type IV collagenase (catalog # 17104–019, Life Technologies) for 25 min at 37 °C in a shaker. 0.5 M EDTA (pH 8) was added to the suspension to stop the enzymatic digestion. After homogenization, the dissociated suspension was passed through a 70 mm cell strainer, washed, and incubated with an anti-mouse CD45 antibody-Alexa Fluor 700 (catalog # 103127, BioLegend, San Diego, CA, USA) for half an hour. After washing, Hoechst (catalog #33258, Invitrogen) was added to the cell suspension. Then, live CD45+ cells were immediately sorted by a Cytek Aurora CS cells sorter and counted under a microscope. Samples with a viability above 85 % and >990 live cells/μl were proceeded with scRAN-seq.

scRNA-Seq was performed by the Iowa Institute of Human Genetics, Genomic Division using the 10× Genomics Chromium X Series Controllers and the Next GEM Single Cell 3′ Kit v3.1 (PN-1000269) by following the manufacturer's (10× Genomics, Pleasanton, CA) recommended protocols (10× Genomics, Pleasanton, CA). Up to 10,000 cells were individually encapsulated along with the 10× GEM code beads using the 10× Genomics Single Cell Chromium iX Controller. Following cDNA synthesis, the oil droplets containing *gem* code beads and nuclei were broken to release the cDNA. Twenty-five percent of the amplified cDNA was used to prepare the dual-indexed (PN-1000215) sequencing libraries. Pooled libraries were sequenced on an Illumina NovaSeq 6000 to give at least 20,000 reads per cell. The bcl sequencing files were converted to the fastq file format using the bcl2fastq program.

2.11. RNA extraction and RNA-sequencing (RNA-seq)

The gingival tissues approximating the ligature were collected and homogenized by a biomasher (catalog # 749625–0030, Kimble, Japan) at the end of the LIP model on day 10 post-ligature placement. Then, RNA was extracted with a miRNeasy mini kit (catalog # 217004, Qiagen, Germany) following the manufacturer's manual. The total RNA quantity and purity were analyzed using a Bioanalyzer 2100 and RNA 6000 Nano LabChip Kit (5067–1511, Agilent, CA, USA). RNA samples passing the quality control (RIN > 7.0) were used to construct the sequencing library. mRNA was purified from the total RNA using Dynabeads Oligo (dT) (Thermo Fisher Scientific, Waltham, MA, USA). After purification, the mRNA was fragmented into short fragments and reverse-transcribed to create the cDNA

by SuperScript II Reverse Transcriptase (catalog # 18064014, Invitrogen), which was then used to synthesize the second-strand DNA. After ligation to the dual-indexed adapter, the ligated DNA fragments were amplified with PCR (8 cycles of denaturation, annealing, and extension). At last, the barcoded DNA fragments were sequenced with 2X150bp paired-end sequencing (PE150) on an Illumina Novaseq™ 6000 platform (Illumina, San Diego, CA, USA) according to the manufacturer's recommended protocol.

2.12. Quantitative real-time PCR analysis

According to the manufacturer's instructions, the isolated RNA was reverse transcribed into cDNA by a SuperScript III kit (catalog # 11755–050, Invitrogen). RT-qPCR was performed using a Taqman universal qPCR system (Applied Biosystem, USA) with gene-specific primer/probes *via* a real-time thermocycler (Bio-Rad Systems, USA). Those gene-specific primer/probes sets included *Selp* (Mm00486048_m1), *Sele* (Mm00441278_m1), *C5ar1* (Mm00500292_m1), *Csf3r* (Mm00432735_m1), *Trem1* ((Mm0127 8455_m1),) *Il18rap* (Mm00516053_m1), *Ctsk* (Mm00484039_m1), *Nfatc1* (Mm01265944_m1), *Dcstamp* (Mm004209236_m1), *Ilb* (Mm0043 4228_m1), *Il17* (Mm00439618_m1), *Il23* (Mm00518984_m1), *Tnfa* (Mm00443258_m1), *Cxcl1* (Mm04207460_m1), *Cxcl2* (Mm0043645 0_m1), *Cxcl5* (Mm00436451_M1), *Inos* (Mm00440502_m1), *Mrc1* (Mm01329362_m1). The transcription level of all targets was first normalized to the CT value of the housekeeping gene *Gapdh* (Mm99999915_g1). The data then was presented as a fold-change of relative quantities to the control samples *via* a $2^{-\Delta\Delta Ct}$ method [37].

2.13. Flow cytometry

On day 6, we collected the ligated gingival tissues from mice to analyze the IFN-β expression and immune cell populations. For the analysis of innate immune cell populations, single-cell suspensions were prepared from the ligated tissues according to a method we previously described [9]. We also used the same method to prepare the cell suspension for the single-cell RNA-seq experiment mentioned above. After enzymatic digestion, physical dissociation, and passing through a 70 μm cell strainer within RPMI 1640 medium, the cells isolated from the mouse gingiva were stained with following markers: anti-mouse CD45-Alex Fluor 700 (catalog # 103127, BioLegend, San Diego, CA), CD11b-VioBright FITC (catalog # 130–113–805, MACS Miltenyi, Gaithersburg, MD, USA), anti-mouse F4/80-APC (catalog # 123115, BioLegend), anti-mouse Ly6G-PerCP (catalog # 127653, BioLegend), anti-mouse CD206-Brilliant Violet 605 (catalog # 141721, BioLegend) and anti-mouse iNOS (NOS2)-PE (catalog # 130–116–422, MACS Miltenyi). An antibody staining panel without the anti-iNOS antibody was performed as fluorescence minus one (FMO) control to help with gating. A Live/Dead fixable Aqua Dead Cell Stain Kit (catalog # L34965, Invitrogen) was used to differentiate live and dead cells. Intracellular markers were stained after fixation and permeation. To test the neutrophil depletion efficiency, cells were stained with Ly-6C-APC (catalog # 560595, BD Biosciences, Franklin Lakes, NJ, USA) and Ly-6G/Ly-6C(Gr-1)-PerCP (catalog # 108425, BioLegend) antibodies in addition to anti-CD45 and anti-CD11b antibodies and the Liev/Dead Fixable Aqua Dead Cell Stain Kit as mentioned above.

For analyzing IL-17 expressing cell populations, ligated gingival tissues and cervical lymph nodes were collected, and the single-cell suspensions were prepared. Cells passing through a 70 μm cell strainer were stimulated for 3 h with 50 ng/ml PMA (catalog # P8139, Sigma-Aldrich) and 2.5 μg/ml ionomycin (catalog # I3909, Sigma-Aldrich) in the presence of 10 μl GolgiPlug (catalog # 555029, BD Biosciences) at 37 °C. After washing, cells were stained with an anti-mouse CD45-Alexa Fluor 700 antibody (catalog # 56–0451–82, Invitrogen), anti-mouse CD3e-PerCP antibody (catalog # 561089, BD Biosciences), anti-mouse CD4-PE-Cy7 (catalog # 100422, BioLegend), anti-mouse FOXP3-BV421 (catalog # 126419, BioLegend), anti-mouse IL-17-BV510 (catalog # 564168, BD Biosciences) and anti-mouse ROR gamma t-PE (catalog # 12–6981–82, eBioscience, San Diego, CA, USA), which was used to verify gated IL-17^+ cells. A Live/Dead Fixable Green Dead Cell Stain kit was used for staining to differentiate live cells from dead ones (catalog # L34969, Thermo Fisher Scientific). An antibody staining panel without the anti-IL-17 antibody was performed as FMO control to help with gating. To identify TCR gd T cells, we stained cells with the anti-mouse TCR g/d- BV421 antibody (catalog # 118119, BioLegend) and anti-mouse TCR b-PE (catalog # 109208, BioLegend) in addition to the anti-CD45, anti-CD3e, and anti-IL-17 antibodies and the Live/Dead Fixable Stain kit. For the *ex vivo* macrophage-T cell co-culture experiment, cells were stained with an anti-mouse CD45-Alexa Fluor 700 antibody, anti-mouse CD3e-PerCP antibody, anti-mouse CD4-PE-Cy7, and anti-mouse IL-17-BV510 antibodies and with a Live/Dead Fixable Green Dead Cell Stain kit, as mentioned above.

Samples were then run through an LSR II Violet flow cytometer (BD Biosciences), and data were analyzed *via* FlowJo 10 software.

2.14. Lactate dehydrogenase (LDH) cytotoxicity assay

According to the manufacturer's instructions, cell viability was assessed using a CyQUANT™ LDH Cytotoxicity Assay kit (catalog # C20300, Invitrogen). BMDMs were seeded in a 96-well plate with 1×10^4 cells/well and the *ex vivo* differentiated osteoclasts were seeded in 96-well plates with 5×10^4 cells/well. The absorbance was measured using a microplate reader (SpectraMax iD3, Molecular Devices) at a wavelength of 490 nm.

2.15. Bioplex multiplex immunoassay and enzyme-linked immunosorbent assay (ELISA)

GCF samples were assayed for inflammatory mediators of IL-1α and IFN-β using a Bio-Plex 200 multiplex format (Bio-Rad Laboratories, Hercules, CA). The concentrations of those GCF mediators were calculated. All key reagents for GCF mediator immunoassays were purchased from R&D Systems. The detailed description of the multiplex immunoassay procedure for GCF mediator analyses in this study was elaborated on previously [38].

Ex vivo differentiated mouse BMDMs were stimulated with LPS (100 ng/ml) with or without the co-treatment of murine IFN-β for 18 h. Cell culture supernatants were collected. The level of CXCL1 (catalog # DY-453–5), CXCL2 (catalog # DY452–05), IL-6 (catalog # DY406–05), IL-1β (catalog # DY401–05), and IL-10 (catalog # DY417–05) was measured by a DuoSet ELISA kit (R&D systems, USA) following the manufacturer's instructions. The supernatant level of IL-17 from the co-culture experiment was also assessed using a DuoSet ELISA kit (catalog # DY-421–05).

2.16. Local delivery of IFN-β in the mouse gingiva

5 μl of 200 ng/μl murine IFN-β (catalog # 8234-MB-010/*CF*, R&D Systems) was locally delivered into the palatal gingiva approximating the ligature placement in each WT mouse through a microinjection syringe (catalog # 7633–01, Hamilton, Reno, NV, USA). PBS served as the control treatment. We started the local delivery of IFN-β on the same day as ligature placement in the LIP model and repeated this local delivery every other day. Samples were collected for analysis on day 10 after ligature placement.

2.17. Bioinformatics analysis and statistics

Preprocessing of single-cell RNA-seq data, such as demultiplexing, barcode assignment, and unique molecular identifier (UMI) quantification, was done using the Cell Ranger pipeline (v7.1.0) provided by 10× Genomics. The reads were aligned to the mouse reference genome prebuilt by 10× Genomics (refdata-gex-mm10–2020-A). Quality control was performed with the following metrics: (1) ambient RNA contamination removal by SoupX (v1.6.2) [39]; (2) doublet detection and removal by DoubletFinder (v2.0.4) [40]; (3) cell-level metric: number of genes ≥500, unique molecular identifier (UMI) counts ≥1000, mitochondrial ratio < 0.1; (4) gene-level metric: genes detected in ≤3 cells in each sample were excluded. Downstream analyses were performed using the Seurat package (v5.0.1) [41]. Specifically, integrative analysis was applied to integrate the same cell types across samples, followed by the identification of marker genes for each cluster, and cell types were then manually annotated based on these marker genes (supplemental Fig. 3 A). Differential gene expression analyses were performed using the Wilcoxon Rank Sum test, and p values were adjusted using Bonferroni correction. Molecular Signatures Database (MSigDB) hallmark gene sets provided in R package msigdbr (v7.5.1) [42] were used for gene set enrichment analysis run by genekitr (v1.2.5) [43].

For bulk RNA-seq analysis, sequenced reads were filtered (merge, trim, cluster) by Cutadapt to get high-quality clean reads, which were then aligned to the mouse reference genome using HISAT2 (https://daehwankimlab.github.io/hisat2/,version:hisat2–2.0.4) package. Analysis of differentially expressed genes was performed by DEseq2 between two different groups. Genes with a parameter of false discovery rate (FDR) below 0.05 and an absolute fold change ≥ 2 were considered differentially expressed genes [44,45]. Differentially expressed genes were then subjected to enrichment analysis of Gene ontology (GO) [46]. Heatmap was performed with ggplot of R in the case.

Clinical data were analyzed using the Mann-Whitney U test, as the distribution of clinical variables is skewed. Murine data are presented as the mean ± SD. Comparisons of alveolar bone loss, numbers of osteoclasts, real-time transcriptomics data, immune cell populations, and ELISA proteomics data were performed using unpaired student's t-test, one-way ANOVA, or two-way ANOVA followed by *post-hoc* pairwise comparisons. $p = 0.05$ was set as the threshold for statistical significance.

3. Results

3.1. GCF levels of IFN-β are negatively associated with clinical periodontitis

We assayed the GCF concentration levels of IFN-β in a subset of the Atherosclerosis Risk in Community (ARIC) subjects, excluding those who were smokers and diabetic and those with potential high risks for cardiovascular diseases by taking cholesterol-reducing medications. We observed that GCF IFN-β levels in "IFN-β high" group, which was defined as above the average GCF IFN-β level of all subjects, were non-significantly associated with less severe periodontitis, which was measured by the extent of all periodontal sites with attachment loss greater than or equal to 3 mm (EALGE3), than the GCF IFN-β levels that were below the average ("IFN-β low" group) (Fig. 1, left panel). However, higher GCF levels of IFN-β were significantly associated with a lower prevalence of attachment loss with ≥3 mm only in the interproximal sites (EALGE3i), which are more vulnerable to periodontitis than other sites (buccal or lingual) of a tooth (Fig. 1, middle panel). We further found that high IFN- β levels were significantly associated with less clinical gingival inflammation, which was measured by the extent of periodontal sites with a gingival index greater than or equal to 1 (EGIGE1), than that in the IFN-β low group (Fig. 1, right panel). We also determined the GCF levels of IL-1α, which is a well-studied proinflammatory cytokine in periodontal disease, in those subjects. We found that higher GCF concentration levels of IL-1α ("IL-1α high" group) were significantly associated with more disease activity in all sites (EALGE3) and in the interproximal sites only (EALGE3i) (Supplemental Fig. 1 A). There was a trend that subjects in the IL-1α high group had more gingival inflammation, as reflected by the EGIGE1 index. Further regression analysis demonstrated that levels of GCF IFN-β were significantly inversely associated with clinical disease measurements of attachment loss at the interproximal sites and clinical gingival inflammation (Supplemental Fig. 1B). In summary, we found that higher levels of IFN-β in GCF were associated with less severe clinical disease phenotypes, including less prevalent attachment loss and gingival inflammation.

3.2. Loss of type I interferon (IFN-I) signaling is associated with more periodontal bone loss in the ligature-induced periodontitis (LIP) model

To characterize the expression pattern of the IFN-I molecules in periodontal disease, we first performed immunohistochemistry (IHC) to stain the IFN-β molecule in human gingival biopsy samples. We found that the expression of IFN-β was more prevalent in the gingival tissue with periodontitis than in the biopsy with periodontal health (Fig. 2A). Both gingival epithelial cells and immune cells that infiltrated into the connective tissue compartment were positively stained for IFN-β (Fig. 2A). We also observed that more IFN-β expression was found in the periodontium of the ligated mice in an LIP model than in the periodontal tissue collected from the non-ligated contralateral control site (Fig. 2B). The induction of the IFN-β expression in the ligated gingival tissue was further confirmed using an *Ifnb1*-YFP reporter mouse strain (*Ifnb*^{mob}) through flow cytometry (Supplemental Fig. 2A and B). To assess the role of IFN-I in periodontal disease, we compared the alveolar bone loss in the global *Ifnar1* knockout mice (*Ifnar1*$^{-/-}$) with that of the wild-type (WT) control mice in the LIP model. Although the alveolar bone level was similar in the non-ligated animals, *Ifnar1*$^{-/-}$ mice manifested significantly more periodontal alveolar bone loss than WT mice

at both the 1st and 2nd molar in the LIP model (Fig. 2C and D). Consistently, the ligated side of *Ifnar1*$^{-/-}$ mice had a significant decrease in the residual alveolar bone volume/total fraction (BV/TV) measurement compared to WT mice (Fig. 2E). We also performed the tartrate-resistant acid phosphatase (TRAP) staining to compare the osteoclast number in the *Ifnar1*$^{-/-}$ mice with that in the WT mice. Significantly more osteoclasts were present in the ligated periodontium of the *Ifnar1*$^{-/-}$ mice than in the WT mice (Fig. 2F and G). These data demonstrate that an integral IFN-I pathway mitigates the periodontal alveolar bone loss in the LIP model.

3.3. Lack of the IFN-I response establishes a unique immune transcriptomic signature in gingiva that sustains an exaggerated inflammatory response in myeloid cells

A more pronounced alveolar bone loss pattern in the ligated *Ifnar1*$^{-/-}$ mice prompted us to compare the immune profile in the local *Ifnar1*$^{-/-}$ gingiva to that of the WT mice. We first determined the early inflammatory infiltrates on day 3 after ligature placement, a stage prior to noticeable bone loss [35], by performing single-cell RNA sequencing (scRNA-seq). We prepared the gingival single-cell suspension pooled from two ligated *Ifnar1*$^{-/-}$ mice and two ligated WT mice separately and sorted out live CD45^{+} immune cells, on which scRNA-seq was performed. After quality control and filtering, we analyzed 4442 cells and 4361 cells from the WT and *Ifnar1*$^{-/-}$ gingival samples, respectively. We identified a total of 13 cell clusters (Fig. 3A). Clusters 7, 8, and 9 expressed common neutrophil markers such as *Cxcr2*, *Ly6g, Lcn2, Camp, and Cd177* to varying degrees [47,48], while clusters 10 and 11 expressed common macrophage transcript markers such as *Mrc1*, *Mafb*, *Arg1*, and *C1qa* at different levels [49]. Detailed cell cluster-defining expression profiles are listed in Supplemental Fig. 3A. We found that the percentage of Cluster-9 (neutrophil-3) in the *Ifnar1*$^{-/-}$ gingiva was more than twofold higher than that in the WT mice (42.8 % *vs.* 20.55 %) and the percentage of Cluster-10 (macrophage-1) in the knockout (KO) mice was also higher than that in the WT mice (9.75 % *vs.* 5.82 %) (Fig. 3B and Supplemental Fig. 3B). We also found a significant transcriptional upregulation with at least a 2-fold increase of genes associated with chemotaxis, including *Cxcl1*, *Cxcl2*, *Cxcl3, Ccl3, Ccl4*, and *C5ar1*, common inflammatory marker genes including *Il1b, Il1a*, and *Tnf (a)*, and those associated with immune function including *Sod2*, *Nos2,* and *Mmp14*, in several myeloid cell clusters (Cluster 7–12) in the *Ifnar1*$^{-/-}$ mouse gingiva as compared to WT samples (Fig. 3C and Supplemental Fig. 3C). Most upregulated genes in the knockout animals were within Clusters-9 and −10. We did not detect the *Ifnb* expression in the scRNA-seq dataset, possibly due to the relatively low expression of *Ifnb* or the limitations of the scRNA-sequencing approach [50,51]. We verified the transcriptional induction of *Ifnb* in CD45^{+} immune cells isolated from the ligated gingiva (data not shown). We performed a pathway analysis to further evaluate the alterations in the biological function supported by those differentially expressed genes. We found several pathways, such as TNFA signaling *via* NF-κB, reactive oxygen species pathway, and the inflammatory response, were significantly upregulated in Cluster-9 and Cluster-10 from the *Ifnar1*$^{-/-}$ mouse gingiva relative to the WT samples (Fig. 3D). In contrast, interferon-α and interferon-γ responses were significantly downregulated in the knockout samples (Fig. 3D).

Next, we assessed the transcriptomic profile at the late stage on day 10 at the end of the LIP model, when bone loss peaked [35], through global RNA sequencing (RNA-seq) using the ligated WT and *Ifnar1*$^{-/-}$ gingiva. We found a total of 236 genes differentially expressed in the ligated gingival samples from the *Ifnar1*$^{-/-}$ mice compared to WT mice, with 131 genes significantly upregulated and 105 genes significantly downregulated (supplementary fig. 3D). We again identified a distinct transcriptomic signature in the *Ifnar1*$^{-/-}$ gingival tissues featured by an upregulation of genes associated with myeloid cell differentiation, recruitment, and activation, including *Trem1, Csf3r, Il18rap, C5ar1, Mmp12, Treml4, Ncf1, Sele, Selp,* and *Lrg1* (Fig. 3E). We further validated the upregulation of several of those inflammatory genes by RT-qPCR using additional independent samples (Fig. 3F). The Gene ontology (GO) analysis demonstrates an enrichment of inflammation-associated biological processes in the ligated *Ifnar1*$^{-/-}$ gingiva compared to the WT tissue (Supplemental Fig. 3E). For example, responses including innate immune response, immune system process, response to bacterium, and scavenger receptor activity were upregulated by the GO analysis. We conclude that the absence of IFN-I signaling unleashed a sustainable hyper-myeloid inflammatory response in the LIP model.

3.4. Deficiency of the IFN-I signaling results in an increased local neutrophil recruitment

The upregulated transcriptional expression of inflammatory genes in the *Ifnar1*$^{-/-}$ mice could be due to more innate immune cells recruited in the ligated gingiva in the knockout mice. To test this hypothesis, we compared the numbers of infiltrating neutrophils ($CD45^+CD11b^+Ly6G^+F4/80^-$) and tissue macrophages ($CD45^+CD11b^+Ly6G^-F4/80^+$) in the ligated *Ifnar1*$^{-/-}$ mouse gingiva with those present in the WT mouse tissue through flow cytometry. We observed a significant increase in neutrophils in the ligated *Ifnar1*$^{-/-}$ mouse gingiva than in the WT tissue (Fig. 4A and B). More $Ly6G^+$ neutrophils stained by IHC in the knockout mouse periodontium than in the WT sample support the flow cytometry data (Supplemental Fig. 4A). However, there was no significant difference in macrophage numbers (Fig. 4A and B). In addition, the ratio of the proinflammatory macrophage phenotype (M1, $NOS2^+$ $CD206^-$ macrophage) and the reparative phenotype (M2, $NOS2^-$ $CD206^+$ macrophage) was not different in the WT murine gingiva as compared to the *Ifanr1*$^{-/-}$ mice (Supplemental Fig. 4B and C).

To further test the hypothesis that unrestrained neutrophil recruitment to the local gingiva was mechanistically responsible for more severe bone loss, we depleted the neutrophils in the *Ifnar1*$^{-/-}$ mice used in the LIP model. The monoclonal depleting antibody 1A8 reduced approximately 60 % and 80 % of neutrophils in the gingival tissue and peripheral blood, respectively (Fig. 4C and Supplemental 4D). Notably, neutrophil depletion significantly mitigated bone loss at the 1st molar compared to mice treated with the isotype control mAb (Fig. 4D and E). The volumetric analysis (BV/TV) further confirmed the reduced bone resorption in the 1A8 treated animals (Fig. 4F). Taken together, these data clearly demonstrate that an intact IFN-I signaling alleviates an excess neutrophil-mediated alveolar bone loss pattern in the LIP model.

3.5. IFN-I signaling inhibits an exuberant inflammatory response and osteoclastogenesis in ex vivo differentiated macrophages

Although we did not observe a quantitative change of macrophages in the gingiva of *Ifnar1*$^{-/-}$ mice, macrophages from the *Ifnar1*$^{-/-}$ mice may harbor a hyperinflammatory phenotype in response to stimuli. To evaluate the effect of IFN-β in the general inflammatory response, we *ex vivo* differentiated bone marrow-derived monocytes (BMDMs) into macrophages, then stimulated the macrophages with LPS in the presence or absence of the IFN-β cotreatment. We found that the *ex vivo* differentiated macrophages from the *Ifnar1*$^{-/-}$ BMDMs secreted significantly more chemokines CXCL1 and CXCL2 than the WT macrophages upon LPS treatment (Fig. 5A and B). Both chemokines are critical for neutrophil recruitment. The IFN-β co-treatment suppressed the LPS-induced chemokine production in the WT macrophages. We verified that the reduced CXCL1 and CXCL2 production was not due to more dead WT cells upon IFN-β treatment (Supplemental fig. 5A). Similarly, IFN-β co-treatment significantly reduced the LPS-stimulated IL-6 production only in the WT cells (Fig. 5C). In addition, *Ifnar1*$^{-/-}$ macrophages secreted significantly more IL-1β than the WT macrophages upon LPS challenge (Fig. 5D). We also evaluated the effect of IFN-β on the secretion of the anti-inflammatory molecule IL-10 and found that the IFN-β co-treatment significantly enhanced the LPS-stimulated IL-10 secretion in WT macrophages. The IL-10 level was significantly less in the *Ifnar1*$^{-/-}$ BMDMs than in WT cells regardless of IFN-β co-treatment (Fig. 5E). Collectively, these results demonstrated that IFN-β dampens an exuberant inflammatory response in macrophages.

We next determined the direct effect of IFN-β in *ex vivo* osteoclast differentiation. We isolated BMDMs from the WT and *Ifnar1*$^{-/-}$ mice and differentiated them into osteoclasts in the presence of GM-CSF and RANKL. We observed that the number of osteoclasts differentiated from the *Ifnar1*$^{-/-}$ BMDMs did not differ from that of the WT cells (Fig. 5F and G). While the IFN-β treatment dramatically reduced the number of osteoclasts differentiated from the WT BMDMs, IFN-β failed to inhibit the osteoclast differentiation in the *Ifnar1*$^{-/-}$ BMDMs (Fig. 5F and G). Additionally, we found that the transcription of several essential genes critical for the osteoclast differentiation program, *Nfatc1, Ctsk1, and Dcstamp*, was drastically inhibited by IFN-β in the WT BMDM differentiation culture (Fig. 5H). We also confirmed that a decreased osteoclast formation in the WT BMDM differentiation culture was not due to reduced cell viability upon IFN-β treatment (Supplemental Fig. 5B). The above data indicate that IFN-β dampens the LPS-elicited inflammatory response in differentiated BMDMs and potently inhibits osteoclastogenesis induced by RANKL.

3.6. IFN-I protects against bone loss by dampening the IL-17-neutrophil axis

We have recently reported that the absence of anti-inflammatory signals such as IL-10 and IL-1RA results in an overactivation of the IL-17 pathway in periodontal tissue, which increases the susceptibility to periodontitis in mice [9,10]. However, the mechanism of the IL-17-mediated pathology in periodontitis with IFN-I deficiency remains unknown. Thus, we first observed the IL-17(A) expression by IHC and found that the IL-17 expression appeared to be elevated in the ligated *Ifnar1*$^{-/-}$ mouse periodontium compared to the WT mouse sample (Fig. 6A). Consistently, significantly more IL-17^{+} cells were detected in the

ligated *Ifnar1*$^{-/-}$ mouse gingiva than in the WT mice through flow cytometry analysis (Fig. 6B and C). In contrast, there was no difference in CD4^{+}FoxP3^{+} regulatory T cells (Treg) in the ligated murine gingiva comparing *Ifnar1*$^{-/-}$ with WT mice (Fig. 6B and C). The ratio of IL-17^{+} cells to Treg was significantly higher in the knockout mouse gingiva than in the WT mouse samples (Fig. 6D). We also found that the increase in IL-17^{+} cells in the *Ifnar1*$^{-/-}$ mice was confined to the gingiva in the LIP model because there was no significant difference in the IL-17^{+} cell number or the ratio of IL-17^{+} to Treg cells in the cervical lymph nodes in the knockout mice as compared with the WT animals (Supplemental Fig. 6A-C).

In our previous report, we found that the transcription of genes closely associated with neutrophil recruitment was significantly reduced in the gingiva of the *Act1*$^{-/-}$ (*Tra3ip2*$^{-/-}$) mice, in which the IL-17 signaling is disrupted [4]. ACT1(TRAF3IP2) is a non-redundant gatekeeping adaptor protein for all IL-17 receptors and mediates the cellular response stimulated by all IL-17 ligands [52,53]. Therefore, we hypothesized that the deficiency of IFN-I unleashes an unconstrained IL-17 response that leads to a neutrophil-mediated inflammatory insult in the LIP model. To test this hypothesis, we generated the *Ifnar1*$^{-/-}$*Act1*$^{-/-}$ deficient mice (double knockout or dKO), in which all IL-17 responses are absent from the *Ifnar1* null mice. We found that *Ifnar1*$^{-/-}$ *Act1*$^{-/-}$ mice manifested significantly less bone loss than the *Ifnar1*$^{-/-}$ mice in the LIP model (Fig. 6E and F). The bone level of the dKO mice was similar to that of the WT littermate control mice. In addition, the alveolar bone loss in *Ifnar1*$^{-/-}$ mice was significantly more than that of the *Act1*$^{-/-}$ littermate controls. We further observed significantly fewer Ly6G^{+} neutrophils in the *Ifnar1*$^{-/-}$*Act1*$^{-/-}$ mice than the *Ifnar1*$^{-/-}$ mice in the ligated gingiva (Fig. 6G and H). Additionally, the transcriptional expression of neutrophil-associated genes such as *Csf3r, C5ar1, Trem1, Il18rap, and Il1b* was also significantly downregulated in the ligated *Ifnar1*$^{-/-}$*Act1*$^{-/-}$ mouse gingiva compared with that of the *Ifnar1*$^{-/-}$ mouse gingiva (Fig. 6I). These data suggested that the type I interferon response plays a protective role in LIP by preventing the overactivation of an IL-17-neutrophil axis.

3.7. Myeloid-specific type I interferon signaling suppresses bone loss and the IL-17$^{+}_{\gamma\delta}$ T cells in gingiva

The *ex vivo* data from BMDMs in Fig. 5 prompted us to hypothesize that the loss of IFN-I signaling in the monocytic cell lineage may account for the major biological effects observed in the global *Ifnar1* knockout mice in the LIP model. To test this hypothesis, we generated myeloid-specific IFNAR1 deficient mice *LysMcre-Ifnar1*$^{fl/fl}$ and compared their bone loss to the control *Ifnar1*$^{fl/fl}$ mice in the LIP model. We found that the *LysMcre-Ifnar1*$^{fl/fl}$ manifested significantly more alveolar bone loss than the control *Ifnar1*$^{fl/fl}$ mice at the 1st molar (Fig. 7A and B). Accordingly, significantly less residual alveolar bone was present in the *LysMcre-Ifnar1*$^{fl/fl}$ mice than in the *Ifnar1*$^{fl/fl}$ mice, indicating mice with the I-IFN deficiency in myeloid cells are more susceptible to bone loss (Fig. 7C). Significantly more TRAP^{+} osteoclasts observed in the ligated gingiva of *LysMcre-Ifnar1*$^{fl/fl}$ mice than those *of Ifnar1*$^{fl/fl}$ controls are consistent with the bone loss data (Fig. 7D and E). Furthermore, the transcription of *Tnfa* and the IL-17-associated cytokine genes *Il17, Il23, and Il1b* was significantly higher in the conditional knockout mouse gingiva than in the control *Ifnar1*$^{fl/fl}$ samples in the LIP model (Fig. 7F). Additionally, the transcriptional expression of

the neutrophil-associated genes *Trem1, C5ar1,* and *Csf3r* (Fig. 7G) and chemokine genes *Cxcl1, Cxcl2, and Cxcl5* was also significantly upregulated in the *LysMcre-Ifnar1* $^{fl/fl}$ mice than in control *Ifnar1* $^{fl/fl}$ mice (Fig. 7H). We also found a significantly higher ratio of *Inos* to *Mrc1* (*Cd206*) transcripts in the conditional knockout gingiva than in the *Ifnar1*$^{fl/fl}$ mice, indicating an M1 phenotypic polarization of the macrophage in the conditional knockout mouse gingiva (Fig. 7I). Additionally, our *ex vivo* co-culture experiment further demonstrated that the LPS-stimulated macrophages derived from the *Ifnar1*$^{-/-}$ BMDMs significantly increased the Th17 polarization in naïve $CD4^+$ T cells as compared with the $CD4^+$ T cells co-cultured with macrophages derived from the WT BMDMs (Fig. 7J and K). The IL-17 level in the co-culture supernatant from the *Ifnar1*$^{-/-}$ BMDM-derived macrophages was significantly higher than that from the WT macrophage T cell co-cultures (Fig. 7L). We found significantly more IL-17^+ cells in the *LysMcre-Ifnar1* $^{fl/fl}$ ligated gingiva than in the control *Ifnar1*$^{fl/fl}$ mouse gingiva (Fig. 7M and N). Further analysis shows that most of those IL-17^+ cells were γδ T cells rather than TCR-αβ Th17 cells. The IL-17^+ $_{γδ}$ T cell population was expanded in the *LysMcre-Ifnar1* $^{fl/fl}$ mouse gingiva compared with control *Ifnar1*$^{fl/fl}$ mice (Fig. 7M and N). In summary, these data indicate that the monocyte-specific type I interferon response dampens the alveolar bone loss in the LIP model by restricting an IL-17^+ $_{γδ}$ T cell expansion and periodontal inflammation.

3.8. Local delivery of IFN-β alleviates alveolar bone resorption in the LIP model

The anti-inflammatory and anti-osteoclastogenic effects of IFN-β in *ex vivo* differentiated BMDMs in Fig. 5 prompted us to further investigate the *in vivo* effect of IFN-β in the LIP model. The alveolar bone loss was compared in mice that received the local delivery of IFN-β into the palatal gingiva with mice treated with PBS. The locally delivered IFN-β mitigated alveolar bone loss in the palatal side of the 2nd molar (Fig. 8A and B). The BV/TV was significantly higher in the IFN-β-treated animals than those with the PBS treatment (Fig. 8C). $TRAP^+$ osteoclasts were significantly fewer in the IFN-β-treated than in the PBS-treated mice (Fig. 8D and E). The transcriptional analysis in the ligated gingiva also shows that the transcriptional expression of those inflammatory genes that were upregulated in the conditional or global *Ifnar1* knockout mouse gingiva, including *Csf3r, Il1b, Trem1, Cxcl1, Il18rap,* and *Tnfa*, was significantly dampened in the IFN-β-treated group as compared to the PBS-treated group (Fig. 8F). The transcription of *Il17*a was also decreased in the IFN-β-treated mice. To further test the hypothesis that the integrity of IFN-I inhibits an IL-17-neutrophil axis to reduce alveolar bone loss, we compared the neutrophil and IL-17+ cell populations in the mouse gingiva between the PBS and IFN-β treatments through flow cytometry. We found a trend of decrease in neutrophil recruitment in mouse gingiva treated with IFN-β compared to those treated with PBS (Supplemental Fig. 7 A and 7B). Similarly, the percentage of IL-17^+ cells in the mouse gingiva was significantly less in the IFN-β treatment than in the PBS treatment (Supplemental Figs. 7C and 7D). These data confirm that local IFN-β treatment mitigated alveolar bone loss by inhibiting osteoclast differentiation and the inflammatory response in the LIP model.

4. Discussion

Our association analysis of the GCF IFN-β level with clinical disease activities supported an anti-inflammatory role of IFN-I in periodontitis. In high GCF IFN-β group, periodontitis and gingival inflammation were less severe than those with lower IFN-β secretion (Fig. 1 and Supplemental Fig. 1C). Such an inverse relationship between the level of IFN-β and clinical indices was contrasted with a positive association between the disease phenotype and the level of IL-1α [54–57]. Although other studies appeared to support our data [24], the inverse association between IFN-I molecules and periodontal disease needs to be further validated in an independent subject pool with a large sample size similar to the present study. In addition, other IFN-I members in GCF samples, especially IFN-α, also need to be compared among people with different periodontal status.

Surprisingly, the mechanistic role of the IFN-I molecules in periodontal disease is scarce. Here, we reported that the IFN-I signaling thwarts an exaggerated inflammatory response in myeloid cells in the LIP model, which readily incurs more severe local inflammation than the periodontal bacteria-induced bone loss model [9]. Our scRNA-sequencing data at the initial stage and bulk RNA-sequencing data at the end of the LIP model demonstrated a more inflammatory profile in the *Ifnar1*$^{-/-}$ mouse gingival tissue than in the WT samples. This anti-inflammatory response by IFN-α/β molecule is echoed by its therapeutic effect in treating MS [58]. Additionally, IFN-β upregulates the IL-10 expression, a hallmark of effective IFN-β treatment in MS patients [59]. Consistent with this finding, we observed an upregulation of IL-10 in BMDMs by IFN-β, while IFN-β inhibited the LPS-stimulated IL-6, IL-1β, and chemokine expression (Fig. 5). The inhibitory effect of INF-β in BMDMs stimulated by a potent inflammation inducer, *E. coli* LPS, was similar to the published data [60]. However, IFNs-I may play a pathogenic role in SLE by enhancing the expression of MHC class II molecules, CD80, and CD86 in dendritic cells in systemic lupus erythematosus (SLE) patients [16]. Therefore, it appears that the precise role of the IFN-I pathway is disease-specific and is also determined by the major cell types involved.

The duality of monocytes that serve as precursors of both macrophages and osteoclasts prompted us to investigate the role of the IFN-I pathway in monocytes in periodontitis. Our data and other reports have shown that IFN-α/β can directly inhibit RANKL-induced osteoclastogenesis. IFN-β can stimulate the expression of the inducible nitric oxide (NO) synthase (iNOS), which releases NO, a molecule that inhibits osteoclast differentiation and bone resorption [21,61,62]. The IFN-I signaling in monocytes also inhibited the inflammation-promoted bone resorption. The conditional *Ifnar1* KO mice (*LysMcre-Ifnar1*$^{fl/fl}$) manifested significantly more bone loss by upregulating the transcription of several innate immunity genes such as *C5ar1*, *Trem1*, and *Csf3r* that were overlapped with those observed in the global *Ifnar1*$^{-/-}$ mouse gingiva (Figs. 3 and 7) and several neutrophil-specific chemokine genes, which led to excess neutrophil recruitment in gingiva. Here, we provided substantial evidence to support that the protective effect of IFN-I in periodontal bone loss is mainly due to the coupling of the anti-osteoclastogenic and inflammation-suppressing activity of the IFN-I signaling in monocytes.

The specific role of the IL-17 response downstream to the type I interferon pathway is disease-dependent. IFN-I-mediated IL-17 inhibition appears to play a deleterious role in specific bacterial infections. For example, the resistance to *Francisella novicida* infection in the *Ifnar1*$^{-/-}$ mice was associated with an expansion of IL-17^{+} TCR γδ T cells [63]. In a separate study, Shahangian et al. reported that the *Ifnar1*$^{-/-}$ mice were more resistant to a post-influenza *Streptococcus pneumoniae* lung infection than wild-type mice [64]. The improved disease activity in *Ifnar1*$^{-/-}$ mice was due to a moderate increase in the CXCL1/KC-mediated neutrophil infiltration in the airway, which defended the lung tissue against the *S. pneumoniae* infection. We previously showed that the *Act1*$^{-/-}$ (*Traf3ip2*$^{-/-}$) mice were prone to periodontal bone loss upon *P. gingivalis* oral infection and concluded that the integrity of a baseline IL-17-mediated neutrophil response enhanced host defense against *P. gingivalis* [4]. However, in the present study, the progressive bone loss phenotype in the LIP model, which was induced by a dramatic neutrophil influx in response to a rapid accumulation of non-specific bacteria, is in sharp contrast to the disease induced by oral inoculation of specific pathogens, such as *P. gingivalis*, which usually elicits more subdued inflammation and subtle bone loss than the LIP model. A drastic influx of neutrophils in gingiva mediated by a TCR γδ T cell-mediated hyper-IL-17 response in either global *Ifnar1*$^{-/-}$ or monocyte-specific *LyzMCre-Ifnar1*$^{fl/fl}$ mice appeared to be destructive in an inflammation-intensive disease model in our study. Our *ex vivo* co-culture model (Fig. 7), which mimics the local IL-17 competent T cell response in the LIP model, also strongly supported that an intact IFN-I pathway inhibits the secretion of cytokine signals required for a Th17 T cell polarization and IL-17 production. Therefore, the effect of IFNs-I in mitigating an IL-17-neutrophil axis is determined by the etiological agent and is model-specific.

In this study, we used double KO (*Ifnar1*$^{-/-}$/*Act1*$^{-/-}$) to test the hypothesis that in the absence of Type I IFN an excess IL-17-neutrophil axis contributes to the dramatic bone loss (Fig. 6). The obliteration of a universal non-redundant IL-17R adaptor blocks the signaling of all IL-17 family ligands. Although the *Il17a*$^{-/-}$ knockout mice could be used to generate the double knockout (*Ifnar1*$^{-/-}$/*Il17a*$^{-/-}$) to test this hypothesis, the knockout of *Act1*$^{-/-}$ at the adaptor level would avoid any residual IL-17 signaling event due to the redundancy of IL-17 ligand family. To further test this hypothesis, we performed in-depth molecular and cellular analysis in the LIP model with local IFN-β administration (Fig. 8 and Supplemental Fig. 7). Both the transcriptomic and flow cytometry data support our hypothesis.

We observed that an early exaggerated inflammatory response in myeloid cells in the ligated gingiva was sustained into the late stage. In the scRNA-seq data, we observed that the number of IL-17^{+} $_{\gamma\delta}$ T cells was similar between the two genotypes of mice on day 3. However, more IL-17^{+} cells, especially IL-17^{+} $_{\gamma\delta}$ T cells, were identified in the *Ifnar1* knockout mice later in the LIP mode. The IL-17^{+} $_{\gamma\delta}$ T cell expansion perpetuated the initial stage of gingival inflammation, which may be mediated through an IL-17-independent mechanism, to the end of the model. The hyper-response to inflammatory stimulus in *Ifnar1*$^{-/-}$ macrophages (Fig. 5) likely contributed to the exaggerated early neutrophil recruitment. The involvement of IL-17-secreting γδ T cells in inflammatory tissue damage only at a later disease stage was also reported in the ischemic injury in the central nervous

system [65]. Therefore, the late participation of IL-17^{+} $_{\gamma\delta}$ T cells continues to recruit neutrophils and preserve a damaging inflammatory response in tissues.

There are several limitations to this report. First, we did not determine the role of IFN-I in the *P. gingivalis*-induced periodontitis model. Using a neutralizing antibody to block the IFNAR1 receptor, Mizraji et al. found that the antibody treatment ameliorated the bone loss upon *P. gingivalis* oral challenge compared to no treatment. The opposite effect of the IFN-I response from this study is very likely attributable to the models and the etiology, as we discussed above. It would be desirable to use the *Ifnar1* knockout or conditional knockout animals to validate the mechanism identified in the pathogen-induced periodontitis model. In addition, we did not characterize the specific activity of IFNs-I in cells other than monocytes. IFNAR1 is widely expressed in most cell types including immune and non-immune cells. A plethora of studies have demonstrated the role of dendritic cell-specific IFN-I signaling in infectious and inflammatory diseases [66–68]. Although we did not observe a difference in the percentage of dendritic cells in the LIP model from the scRNA-seq data, we cannot rule out the possibility that the IFN-I pathway in dendritic cells is involved in periodontitis.

5. Conclusions

In summary, we found that the level of IFN-β was inversely associated with the severity of periodontitis and periodontal inflammation in subjects enrolled in a national study cohort. In a ligature-induced periodontitis model using global and conditional *Ifnar1* knockout mice, we identified a novel anti-inflammatory role of type I interferon pathway in monocytic cells in mitigating alveolar bone loss by preventing overactivation of an IL-17- neutrophil axis in the periodontal tissue.

Supplementary Material

Refer to Web version on PubMed Central for supplementary material.

Acknowledgements

We sincerely thank the staff and participants of the ARIC study for their contributions. We thank Dr. Ulrich Siebenlist at National Institute of Allergy and Infectious Diseases for providing *Traf3ip2(Act1, CISK)*$^{-/-}$ and wild type control animals. The authors would like to acknowledge the use of the University of Iowa Central Microscopy Research Facility, a core resource supported by the University of Iowa Vice President for Research, and the Carver College of Medicine. We also would like to acknowledge the Small Animal Imaging Core Facility for the micro-CT data. Data presented herein were obtained at the Genomics Division of the Iowa Institute of Human Genetics which is supported, in part, by the University of Iowa Carver College of Medicine. The data presented herein were obtained at the Flow Cytometry Facility, which is a Carver College of Medicine/Holden Comprehensive Cancer Center core research facility at the University of Iowa. The facility is funded through user fees and the generous financial support of the Carver College of Medicine, Holden Comprehensive Cancer Center, and Iowa City Veteran's Administration Medical Center.

Funding

The Atherosclerosis Risk in Communities (ARIC) Study is carried out as a collaborative study supported by National Heart, Lung, and Blood Institute contracts (HHSN268201100005C, HHSN268201100006C, HHSN268201100007C, HHSN268201100008C, HHSN26820110000 9C, HHSN268201100010C, HHSN268201100011C, and HHSN2682 01100012C), R01HL087641, R01HL59367, and R01HL086694; National Human Genome Research Institute contract U01HG004402; National Institutes of Health contract HHSN268200625226C; National Institute of Environmental Health Sciences grant P30ES010126; and National

Institute of Dental and Craniofacial Research grants R01DE11551, R01DE021418. This research was also funded by NIH grants R01 DE032307 (S.Z.), R01 DE026728 and R01 DE030691 (Y.L. L.), and R01 DE032830 (J.T.M). This study was also partially supported by a Colgate Award for Research Excellence (CARE) (S.Z).

Data availability

The data supporting this report's findings are available from the corresponding author upon reasonable request.

Abbreviations

IFN-I	type I interferon
IL	interleukin
IFNAR	interferon-α receptor
GCF	gingival crevicular fluid
LIP	ligature-induced periodontitis
ARIC	Atherosclerosis Risk in Communities
BOP	bleeding on robing
PD	probing depth
AL	attachment level
EALGE3	extent of attachment loss greater than or equal to 3 mm
EGIGE1	extent of gingival index greater than or equal to 1
μCT	micro-computed tomography
EYFP	enhanced yellow fluorescent protein
TRAF3IP2/ACT1	TNF receptor-associated factor 3 interacting protein 2
TRAP	tartrate-resistant acid phosphatase
BMDM	bone marrow-derived monocytic cells
CD	cluster of differentiation
LPS	lipopolysaccharide
TCR	T-cell receptor
M-CSF	macrophage-colony stimulating factor
RANKL	receptor activator of nuclear factor Kappa B ligand
scRNA-seq	single-cell RNA-sequencing
BV/TV	bone volume/total fraction

References

[1]. Fawzy El-Sayed KM, Cosgarea R, Sculean A, Doerfer C. Can vitamins improve periodontal wound healing/regeneration? Periodontol 2000. 2023. doi:10.1111/prd.12513.

[2]. Silva LM, Divaris K, Bugge TH, Moutsopoulos NM, Plasmin-mediated fibrinolysis in periodontitis pathogenesis, J. Dent. Res 102 (2023) 972–978, 10.1177/00220345231171837. [PubMed: 37506226]

[3]. Hajishengallis G, Chavakis T, Local and systemic mechanisms linking periodontal disease and inflammatory comorbidities, Nat. Rev. Immunol 21 (2021) 426–440, 10.1038/s41577-020-00488-6. [PubMed: 33510490]

[4]. Zhang J, Sun L, Withanage MHH, Ganesan SM, Williamson MA, Marchesan JT, et al. , TRAF3IP2-IL-17 Axis strengthens the gingival defense against pathogens, J. Dent. Res 102 (2023) 103–115, 10.1177/00220345221123256. [PubMed: 36281065]

[5]. Zhang S, Philips KH, Moss K, Wu D, Adam HS, Selvin E, et al. , Periodontitis and risk of diabetes in the atherosclerosis risk in communities (ARIC) study: a BMI-modified association, J. Clin. Endocrinol. Metab 106 (2021), 10.1210/clinem/dgab337e3546-e58.

[6]. Leng Y, Hu Q, Ling Q, Yao X, Liu M, Chen J, et al. , Periodontal disease is associated with the risk of cardiovascular disease independent of sex: a meta-analysis, Front Cardiovasc Med. 10 (2023) 1114927, 10.3389/fcvm.2023.1114927. [PubMed: 36923959]

[7]. Garlet GP, Destructive and protective roles of cytokines in periodontitis: a reappraisal from host defense and tissue destruction viewpoints, J. Dent. Res 89 (2010) 1349–1363, 10.1177/0022034510376402. [PubMed: 20739705]

[8]. Hajishengallis G, Korostoff JM, Revisiting the Page & Schroeder model: the good, the bad and the unknowns in the periodontal host response 40 years later, Periodontol 2017 (75) (2000) 116–151, 10.1111/prd.12181.

[9]. Sun L, Girnary M, Wang L, Jiao Y, Zeng E, Mercer K, et al. , IL-10 dampens an IL-17-mediated periodontitis-associated inflammatory network, J. Immunol 204 (2020) 2177–2191, 10.4049/jimmunol.1900532. [PubMed: 32169848]

[10]. Zhang J, Wang AX, Wu Y, Zhang S, IL-1 receptor antagonist (IL-1RA) suppresses a hyper-IL-17 response-mediated bone loss in a murine experimental periodontitis, Arch. Oral Biol 144 (2022) 105555, 10.1016/j.archoralbio.2022.105555. [PubMed: 36191445]

[11]. Boxx GM, Cheng G, The roles of type I interferon in bacterial infection, Cell Host Microbe 19 (2016) 760–769, 10.1016/j.chom.2016.05.016. [PubMed: 27281568]

[12]. Holicek P, Guilbaud E, Klapp V, Truxova I, Spisek R, Galluzzi L, et al. , Type I interferon and cancer, Immunol. Rev 321 (2024) 115–127, 10.1111/imr.13272. [PubMed: 37667466]

[13]. McNab F, Mayer-Barber K, Sher A, Wack A, O'Garra A, Type I interferons in infectious disease, Nat. Rev. Immunol 15 (2015) 87–103, 10.1038/nri3787. [PubMed: 25614319]

[14]. Haller O, Arnheiter H, Gresser I, Lindenmann J, Virus-specific interferon action., Protection of newborn mx carriers against lethal infection with influenza virus, J. Exp. Med 154 (1981) 199–203, 10.1084/jem.154.1.199. [PubMed: 6166723]

[15]. González-Navajas JM, Lee J, David M, Raz E, Immunomodulatory functions of type I interferons, Nat. Rev. Immunol 12 (2012) 125–135, 10.1038/nri3133. [PubMed: 22222875]

[16]. Blanco P, Palucka AK, Gill M, Pascual V, Banchereau J, Induction of dendritic cell differentiation by IFN-alpha in systemic lupus erythematosus, Science 294 (2001) 1540–1543, 10.1126/science.1064890. [PubMed: 11711679]

[17]. Jego G, Palucka AK, Blanck JP, Chalouni C, Pascual V, Banchereau J, Plasmacytoid dendritic cells induce plasma cell differentiation through type I interferon and interleukin 6, Immunity 19 (2003) 225–234, 10.1016/s1074-7613(03)00208-5. [PubMed: 12932356]

[18]. Prinz M, Schmidt H, Mildner A, Knobeloch KP, Hanisch UK, Raasch J, et al. , Distinct and nonredundant in vivo functions of IFNAR on myeloid cells limit autoimmunity in the central nervous system, Immunity 28 (2008) 675–686, 10.1016/j.immuni.2008.03.011. [PubMed: 18424188]

[19]. Guo B, Chang EY, Cheng G, The type I IFN induction pathway constrains Th17-mediated autoimmune inflammation in mice, J. Clin. Invest 118 (2008) 1680–1690, 10.1172/jci33342. [PubMed: 18382764]

[20]. Shinohara ML, Kim JH, Garcia VA, Cantor H, Engagement of the type I interferon receptor on dendritic cells inhibits T helper 17 cell development: role of intracellular osteopontin, Immunity 29 (2008) 68–78, 10.1016/j.immuni.2008.05.008. [PubMed: 18619869]

[21]. Takayanagi H, Kim S, Matsuo K, Suzuki H, Suzuki T, Sato K, et al. , RANKL maintains bone homeostasis through c-Fos-dependent induction of interferon-beta, Nature 416 (2002) 744–749, 10.1038/416744a. [PubMed: 11961557]

[22]. Kwon Y, Park OJ, Kim J, Cho JH, Yun CH, Han SH, Cyclic dinucleotides inhibit osteoclast differentiation through STING-mediated interferon-beta signaling, J. Bone Miner. Res 34 (2019) 1366–1375, 10.1002/jbmr.3701. [PubMed: 30779854]

[23]. MacLauchlan S, Kushwaha P, Tai A, Chen S, Manning C, Swarnkar G, et al. , STING-dependent interferon signatures restrict osteoclast differentiation and bone loss in mice, Proc. Natl. Acad. Sci. USA 120 (2023) e2210409120, 10.1073/pnas.2210409120.

[24]. Acar B, Cagdas D, Tan C, Ozbek B, Yaz I, Yildirim YD, et al. , Evaluation of periodontal status and cytokine/chemokine profile of GCF in patients with severe congenital neutropenia, Odontology 109 (2021) 474–482, 10.1007/s10266-020-00565-1. [PubMed: 33159599]

[25]. Prabhu A, Michalowicz BS, Mathur A, Detection of local and systemic cytokines in adult periodontitis, J. Periodontol 67 (1996) 515–522, 10.1902/jop.1996.67.5.515. [PubMed: 8724710]

[26]. Mizraji G, Nassar M, Segev H, Sharawi H, Eli-Berchoer L, Capucha T, et al. , Porphyromonas gingivalis promotes unrestrained type I interferon production by dysregulating TAM signaling via MYD88 degradation, Cell Rep. 18 (2017) 419–431, 10.1016/j.celrep.2016.12.047. [PubMed: 28076786]

[27]. Ito A, Isogai E, Yoshioka K, Sato K, Himeno N, Gotanda T, Ability of orally administered IFN-alpha4 to inhibit naturally occurring gingival inflammation in dogs, J. Vet. Med. Sci 72 (2010) 1145–1151, 10.1292/jvms.09-0201. [PubMed: 20424396]

[28]. Nomura R, Inaba H, Yasuda H, Shirai M, Kato Y, Murakami M, et al. , Inhibition of Porphyromonas gulae and periodontal disease in dogs by a combination of clindamycin and interferon alpha, Sci. Rep 10 (2020) 3113, 10.1038/s41598-020-59730-9. [PubMed: 32080231]

[29]. Loe H, Silness J. PERIODONTAL DISEASE IN PREGNANCY. I. PREVALENCE AND SEVERITY. Acta Odontol. Scand 1963;21:533–51. doi:10.3109/00016356309011240. [PubMed: 14121956]

[30]. Löe H, The gingival index, the plaque index and the retention index systems, J. Periodontol 38 (Suppl) (1967) 610–616, 10.1902/jop.1967.38.6.610.

[31]. Elter JR, Champagne CM, Offenbacher S, Beck JD, Relationship of periodontal disease and tooth loss to prevalence of coronary heart disease, J. Periodontol 75 (2004) 782–790, 10.1902/jop.2004.75.6.782. [PubMed: 15295942]

[32]. Marchesan JT, Moss K, Morelli T, Teles FR, Divaris K, Styner M, et al. , Distinct microbial signatures between periodontal profile classes, J. Dent. Res 100 (2021) 1405–1413, 10.1177/00220345211009767. [PubMed: 33906500]

[33]. Champagne CM, Buchanan W, Reddy MS, Preisser JS, Beck JD, Offenbacher S, Potential for gingival crevice fluid measures as predictors of risk for periodontal diseases, Periodontol 2003 (31) (2000) 167–180, 10.1034/j.1600-0757.2003.03110.x.

[34]. Scheu S, Dresing P, Locksley RM, Visualization of IFNbeta production by plasmacytoid versus conventional dendritic cells under specific stimulation conditions in vivo, Proc. Natl. Acad. Sci. USA 105 (2008) 20416–20421, 10.1073/pnas.0808537105. [PubMed: 19088190]

[35]. Marchesan J, Girnary MS, Jing L, Miao MZ, Zhang S, Sun L, et al. , An experimental murine model to study periodontitis, Nat. Protoc 13 (2018) 2247–2267, 10.1038/s41596-018-0035-4. [PubMed: 30218100]

[36]. Zhu J, Cao J, Liesz A, Roth S, A macrophage-T cell coculture model for severe tissue injury-induced T cell death, STAR Protoc. 2 (2021) 100983, 10.1016/j.xpro.2021.100983. [PubMed: 34927092]

[37]. Livak KJ, Schmittgen TD, Analysis of relative gene expression data using real-time quantitative PCR and the 2(-Delta Delta C(T)) method, Methods 25 (2001) 402–408, 10.1006/meth.2001.1262. [PubMed: 11846609]

[38]. Offenbacher S, Barros S, Mendoza L, Mauriello S, Preisser J, Moss K, et al. , Changes in gingival crevicular fluid inflammatory mediator levels during the induction and resolution of experimental gingivitis in humans, J. Clin. Periodontol 37 (2010) 324–333, 10.1111/j.1600-051X.2010.01543.x. [PubMed: 20447255]

[39]. Young MD, Behjati S, SoupX removes ambient RNA contamination from droplet-based single-cell RNA sequencing data, Gigascience (2020) 9, 10.1093/gigascience/giaa151.

[40]. McGinnis CS, Murrow LM, Gartner ZJ, DoubletFinder: doublet detection in single-cell RNA sequencing data using artificial nearest neighbors, Cell Syst. 8 (329–37) (2019) e4, 10.1016/j.cels.2019.03.003.

[41]. Hao Y, Stuart T, Kowalski MH, Choudhary S, Hoffman P, Hartman A, et al. , Dictionary learning for integrative, multimodal and scalable single-cell analysis, Nat. Biotechnol 42 (2024) 293–304, 10.1038/s41587-023-01767-y. [PubMed: 37231261]

[42]. Subramanian A, Tamayo P, Mootha VK, Mukherjee S, Ebert BL, Gillette MA, et al. , Gene set enrichment analysis: a knowledge-based approach for interpreting genome-wide expression profiles, Proc. Natl. Acad. Sci. USA 102 (2005) 15545–15550, 10.1073/pnas.0506580102. [PubMed: 16199517]

[43]. Liu Y, Li G, Empowering biologists to decode omics data: the Genekitr R package and web server, BMC Bioinformatics. 24 (2023) 214, 10.1186/s12859-023-05342-9. [PubMed: 37221491]

[44]. Sahraeian SME, Mohiyuddin M, Sebra R, Tilgner H, Afshar PT, Au KF, et al. , Gaining comprehensive biological insight into the transcriptome by performing a broad-spectrum RNA-seq analysis, Nat. Commun 8 (2017) 59, 10.1038/s41467-017-00050-4. [PubMed: 28680106]

[45]. Love MI, Huber W, Anders S, Moderated estimation of fold change and dispersion for RNA-seq data with DESeq2, Genome Biol. 15 (2014) 550, 10.1186/s13059-014-0550-8. [PubMed: 25516281]

[46]. Gene Ontology C., Gene ontology consortium: going forward, Nucleic Acids Res. 43 (2015) D1049–D1056, 10.1093/nar/gku1179. [PubMed: 25428369]

[47]. Goldschmeding R, van Dalen CM, Faber N, Calafat J, Huizinga TW, van der Schoot CE, et al. , Further characterization of the NB 1 antigen as a variably expressed 56–62 kD GPI-linked glycoprotein of plasma membranes and specific granules of neutrophils, Br. J. Haematol 81 (1992) 336–345, 10.1111/j.1365-2141.1992.tb08237.x. [PubMed: 1382544]

[48]. Evrard M, Kwok IWH, Chong SZ, Teng KWW, Becht E, Chen J, et al. , Developmental analysis of bone marrow neutrophils reveals populations specialized in expansion, trafficking, and effector functions, Immunity 48 (364–79) (2018) e8, 10.1016/j.immuni.2018.02.002.

[49]. Tu J, Wang D, Zheng X, Liu B, Single-cell RNA datasets and bulk RNA datasets analysis demonstrated C1Q+ tumor-associated macrophage as a major and antitumor immune cell population in osteosarcoma, Front. Immunol 14 (2023) 911368, 10.3389/fimmu.2023.911368. [PubMed: 36814925]

[50]. Haque A, Engel J, Teichmann SA, Lonnberg T, A practical guide to single-cell ¨ RNA-sequencing for biomedical research and clinical applications, Genome Med. 9 (2017) 75, 10.1186/s13073-017-0467-4. [PubMed: 28821273]

[51]. Bibby JA, Agarwal D, Freiwald T, Kunz N, Merle NS, West EE, et al. , Systematic single-cell pathway analysis to characterize early T cell activation, Cell Rep. 41 (2022) 111697, 10.1016/j.celrep.2022.111697. [PubMed: 36417885]

[52]. Qian Y, Liu C, Hartupee J, Altuntas CZ, Gulen MF, Jane-Wit D, et al. , The adaptor Act1 is required for interleukin 17-dependent signaling associated with autoimmune and inflammatory disease, Nat. Immunol 8 (2007) 247–256, 10.1038/ni1439. [PubMed: 17277779]

[53]. Ha HL, Wang H, Pisitkun P, Kim JC, Tassi I, Tang W, et al. , IL-17 drives psoriatic inflammation via distinct, target cell-specific mechanisms, Proc. Natl. Acad. Sci. USA 111 (2014) E3422–E3431, 10.1073/pnas.1400513111. [PubMed: 25092341]

[54]. Thunell DH, Tymkiw KD, Johnson GK, Joly S, Burnell KK, Cavanaugh JE, et al. , A multiplex immunoassay demonstrates reductions in gingival crevicular fluid cytokines following initial

periodontal therapy, J. Periodontal Res 45 (2010) 148–152, 10.1111/j.1600-0765.2009.01204.x. [PubMed: 19602112]

[55]. Tymkiw KD, Thunell DH, Johnson GK, Joly S, Burnell KK, Cavanaugh JE, et al. , Influence of smoking on gingival crevicular fluid cytokines in severe chronic periodontitis, J. Clin. Periodontol 38 (2011) 219–228, 10.1111/j.1600-051X.2010.01684.x. [PubMed: 21198766]

[56]. Javed F, Al-Askar M, Al-Hezaimi K, Cytokine profile in the gingival crevicular fluid of periodontitis patients with and without type 2 diabetes: a literature review, J. Periodontol 83 (2012) 156–161, 10.1902/jop.2011.110207. [PubMed: 21692634]

[57]. Huang W, Wu J, Mao Y, Zhu S, Huang GF, Petritis B, et al. , Developing a periodontal disease antibody array for the prediction of severe periodontal disease using machine learning classifiers, J. Periodontol 91 (2020) 232–243, 10.1002/jper.19-0173. [PubMed: 31397883]

[58]. Teige I, Liu Y, Issazadeh-Navikas S, IFN-beta inhibits T cell activation capacity of central nervous system APCs, J. Immunol 177 (2006) 3542–3553, 10.4049/jimmunol.177.6.3542. [PubMed: 16951313]

[59]. Rudick RA, Ransohoff RM, Peppler R, VanderBrug Medendorp S, Lehmann P, Alam J, Interferon beta induces interleukin-10 expression: relevance to multiple sclerosis, Ann. Neurol 40 (1996) 618–627, 10.1002/ana.410400412. [PubMed: 8871582]

[60]. Yoo CH, Yeom JH, Heo JJ, Song EK, Lee SI, Han MK, Interferon β protects against lethal endotoxic and septic shock through SIRT1 upregulation, Sci. Rep 4 (2014) 4220, 10.1038/srep04220. [PubMed: 24573134]

[61]. Abraham AK, Ramanathan M, Weinstock-Guttman B, Mager DE, Mechanisms of interferon-beta effects on bone homeostasis, Biochem. Pharmacol 77 (2009) 1757–1762, 10.1016/j.bcp.2009.01.007. [PubMed: 19428330]

[62]. Brandi ML, Hukkanen M, Umeda T, Moradi-Bidhendi N, Bianchi S, Gross SS, et al. , Bidirectional regulation of osteoclast function by nitric oxide synthase isoforms, Proc. Natl. Acad. Sci. USA 92 (1995) 2954–2958, 10.1073/pnas.92.7.2954. [PubMed: 7535933]

[63]. Henry T, Kirimanjeswara GS, Ruby T, Jones JW, Peng K, Perret M, et al. , Type I IFN signaling constrains IL-17A/F secretion by gammadelta T cells during bacterial infections, J. Immunol 184 (2010) 3755–3767, 10.4049/jimmunol.0902065. [PubMed: 20176744]

[64]. Shahangian A, Chow EK, Tian X, Kang JR, Ghaffari A, Liu SY, et al. , Type I IFNs mediate development of postinfluenza bacterial pneumonia in mice, J. Clin. Invest 119 (2009) 1910–1920, 10.1172/jci35412. [PubMed: 19487810]

[65]. Wo J, Zhang F, Li Z, Sun C, Zhang W, Sun G, The role of Gamma-Delta T cells in diseases of the central nervous system, Front. Immunol 11 (2020) 580304, 10.3389/fimmu.2020.580304. [PubMed: 33193380]

[66]. Longhi MP, Trumpfheller C, Idoyaga J, Caskey M, Matos I, Kluger C, et al. , Dendritic cells require a systemic type I interferon response to mature and induce CD4+ Th1 immunity with poly IC as adjuvant, J. Exp. Med 206 (2009) 1589–1602, 10.1084/jem.20090247. [PubMed: 19564349]

[67]. Haque A, Best SE, Montes de Oca M, James KR, Ammerdorffer A, Edwards CL, et al. , Type I IFN signaling in CD8- DCs impairs Th1-dependent malaria immunity, J. Clin. Invest 124 (2014) 2483–2496, 10.1172/jci70698. [PubMed: 24789914]

[68]. Phipps-Yonas H, Seto J, Sealfon SC, Moran TM, Fernandez-Sesma A, Interferon-beta pretreatment of conventional and plasmacytoid human dendritic cells enhances their activation by influenza virus, PLoS Pathog. 4 (2008) e1000193, 10.1371/journal.ppat.1000193.

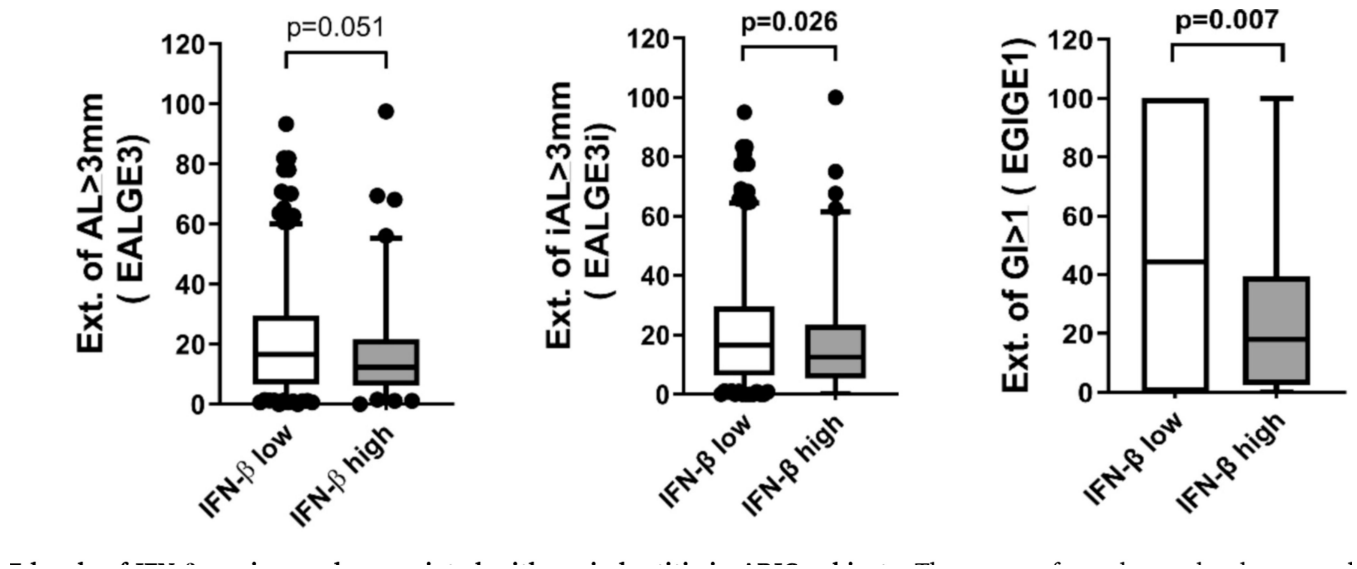

Fig. 1. The GCF levels of IFN-β are inversely associated with periodontitis in ARIC subjects.

The extent of attachment level greater than or equal to 3 mm (EALGE3) in the group of high GCF IFN-β ("IFN-β high"), which was defined by the GCF IFN-β levels at or above the mean level of IFN-β in ARIC subjects, was lower than that of the IFN-β low group, whose GCF IFN-β levels were below the mean (left panel). The lower disease severity measured by the EALGE3 only at the interproximal periodontal sites (EALGE3i) was significantly associated with high GCF IFN-β levels (middle panel). The clinical gingival inflammation measured by the extent of gingival index greater than or equal to 1 (EGIGE1) was significantly lower in the GCF IFN-β high group than in the IFN-β low group (right panel). n = 272–290 in "IFN-β low group"; n = 74–84 in "IFN-β high" group. Data are presented by the median and interquartile range and analyzed by the Mann-Whitney U test.

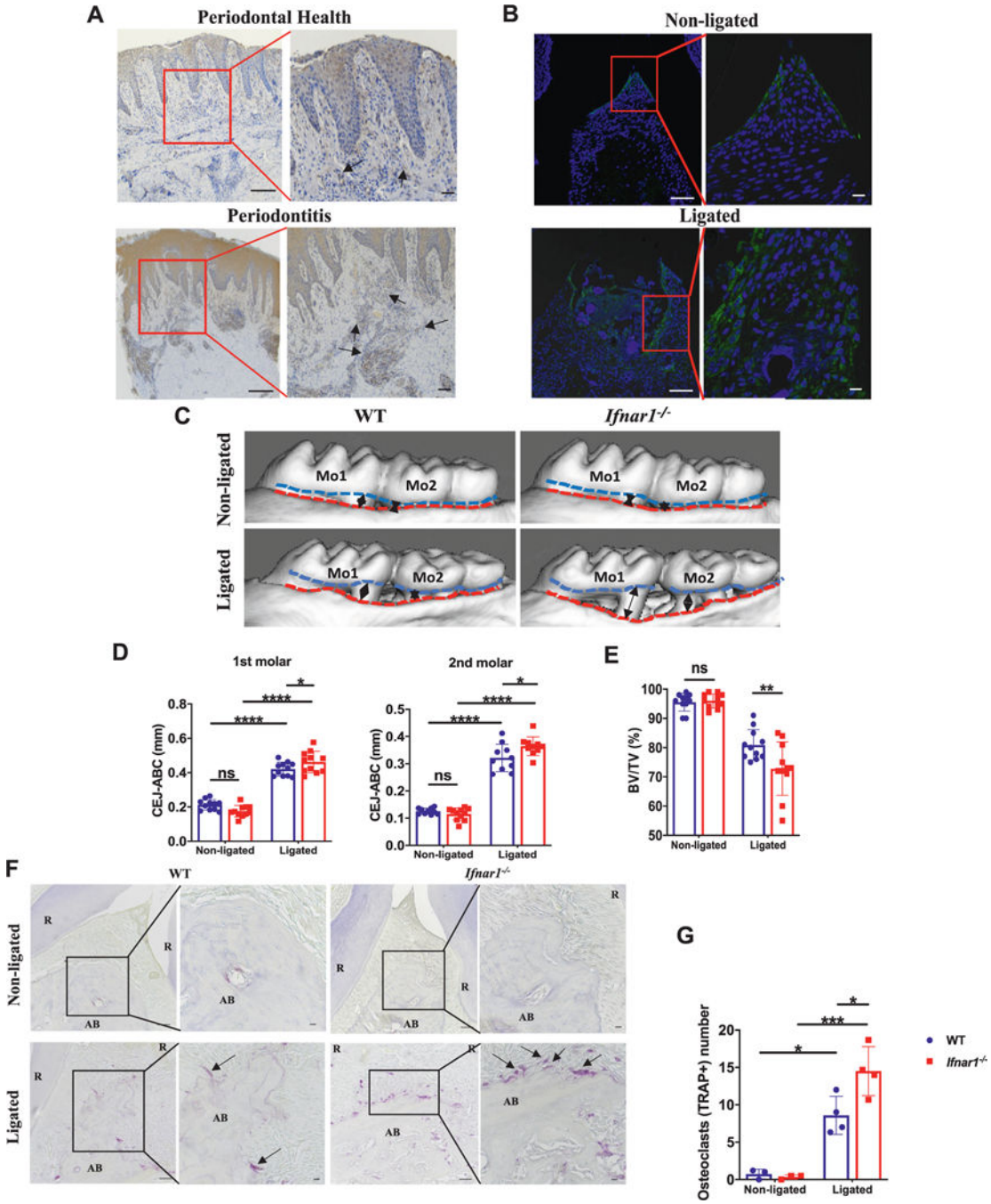

Fig. 2. The type I interferon pathway is indispensable to mitigating the periodontal alveolar bone level in the ligature-induced periodontitis (LIP) model.

Representative immunohistochemistry staining of the IFN-β expression in the gingival biopsy from a participant with periodontal health and a periodontitis patient is shown (A). Representative IFN-β positive cells are pointed by arrows. Representative immunofluorescence staining of the murine IFN-β-EYFP expression in the periodontium from a non-ligated and a ligated periodontal sample in the LIP model is shown (B). Representative micro-computed tomography (micro-CT) images of the periodontal alveolar bone resorption in the non-ligated and ligated side of the LIP model are shown for the

wild-type (WT) and the global *Ifnar1*$^{-/-}$ mice. Mo1 and Mo2 represent the first and second maxillary molar, respectively. The blue dotted line represents the cementum enamel junction (CEJ), while the red dotted line illustrates the alveolar bone crest (ABC) (C). The bone resorption, as quantified by the linear distance between CEJ to ABC at the distal root of Mo1 and the mesial root of Mo2, was compared between WT and *Ifnar1*$^{-/-}$ mice (D). The volumetric analysis calculated by the bone volume fraction (BV/TV) ratio was compared between WT and *Ifnar1*$^{-/-}$ mice (E). n = 10–11/group for the linear and volumetric analysis. Representative histology sections of osteoclasts in the murine periodontium stained by tartrate-resistant acid phosphatase (TRAP) from the non-ligated and ligated side of WT and *Ifnar1*$^{-/-}$ mouse maxillae are shown (F). Arrows indicate representative TRAP^{+} osteoclasts; "R" represents root; "AB" represents alveolar bone. The osteoclast numbers were compared between the WT and *Ifnar1*$^{-/-}$ mouse group (n = 3–4 per group, G). Quantitative data are presented as mean ± SD; two-way ANOVA was applied to the bone resorption analysis and the TRAP^{+} osteoclast quantification data. *$p < 0.05$. **$p < 0.01$, ***$p < 0.001$, ****$p <$ 0.0001, ns: not significant. The scale bar of the left panels of all histology images represents 100 μm; the scale bar of the right panels represents 50 μm.

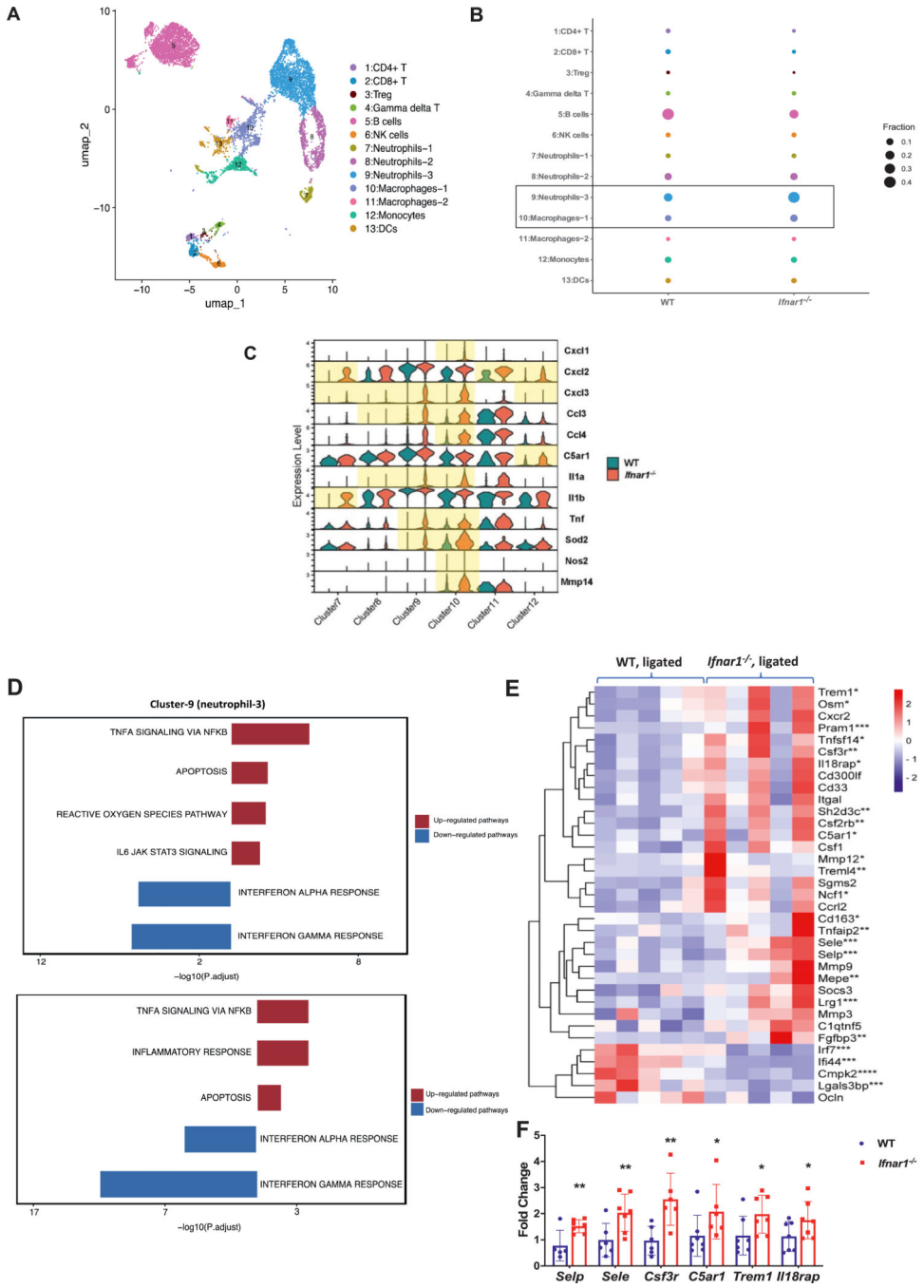

Fig. 3. Deficiency of the IFN-I signaling perpetuates an excess inflammatory response in the gingival myeloid cells.

After ligature placement, the ligated gingiva tissues from the WT mice and *Ifnar1*$^{-/-}$ mice were harvested on Day 3. Live CD45^{+} infiltrating immune cells were sorted *via* FACS (fluorescence-activated cell sorting), pooled based on the genotype (n = 2 mice/ genotype), and subjected to downstream single-cell RNA sequencing. 4442 cells from the WT gingiva and 4361 cells from the *Ifnar1*$^{-/-}$ tissue were used to integrate for UMAP cell cluster analysis. 13 cell clusters were resolved through the R Seurat package (v5.0.1) (A). The composition of each cluster of cells is shown for both WT and *Ifnar1*$^{-/-}$ gingival samples

(B). The transcriptional expression of inflammatory genes, including chemokines *Cxcl1, Cxcl2, Cxcl3, Ccl3*, and *Ccl4* and chemotaxis gene *C5ar1*, cytokines *Il1a, Il1b*, and *Tnf(a),* and immune function *Sod2, Nos2*, and *Mmp14,* is shown in the violin plot for each innate immunity cell cluster. Shaded genes indicate a 2-fold or more upregulation in the *Ifnar1*$^{-/-}$ sample with significance after adjusting the *p*-value (adj-p < 0.05, C). Up-regulated and down-regulated pathways in the *Ifnar1*$^{-/-}$ sample analyzed using genes with ≥2-fold change with significance are shown for Cluster-9 (neutrophil-3, upper panel) and Cluster-10 (macrophage-1, lower panel) (D). After ligature placement, the ligated gingival tissues were collected from WT (*n* = 5) and *Ifnar1*$^{-/-}$ mice (n = 5) on Day 10. The RNA was isolated from the tissue and sequenced. The heatmap shows the transcriptional expression of genes between the ligated WT and *Ifnar1*$^{-/-}$ tissue samples (E). Asterisks indicate significantly expressed genes with at least a 2-fold change difference. The transcription of several selected inflammatory genes was further independently validated with real-time quantitative PCR (RT-qPCR) using additional ligated tissue samples from both WT and *Ifnar1*$^{-/-}$ mice (n = 5–7/group, F). The fold change difference was analyzed by the unpaired *t-test*. * p < 0.05; **p < 0.01, ***p < 0.001, ****$p < 0.0001$.

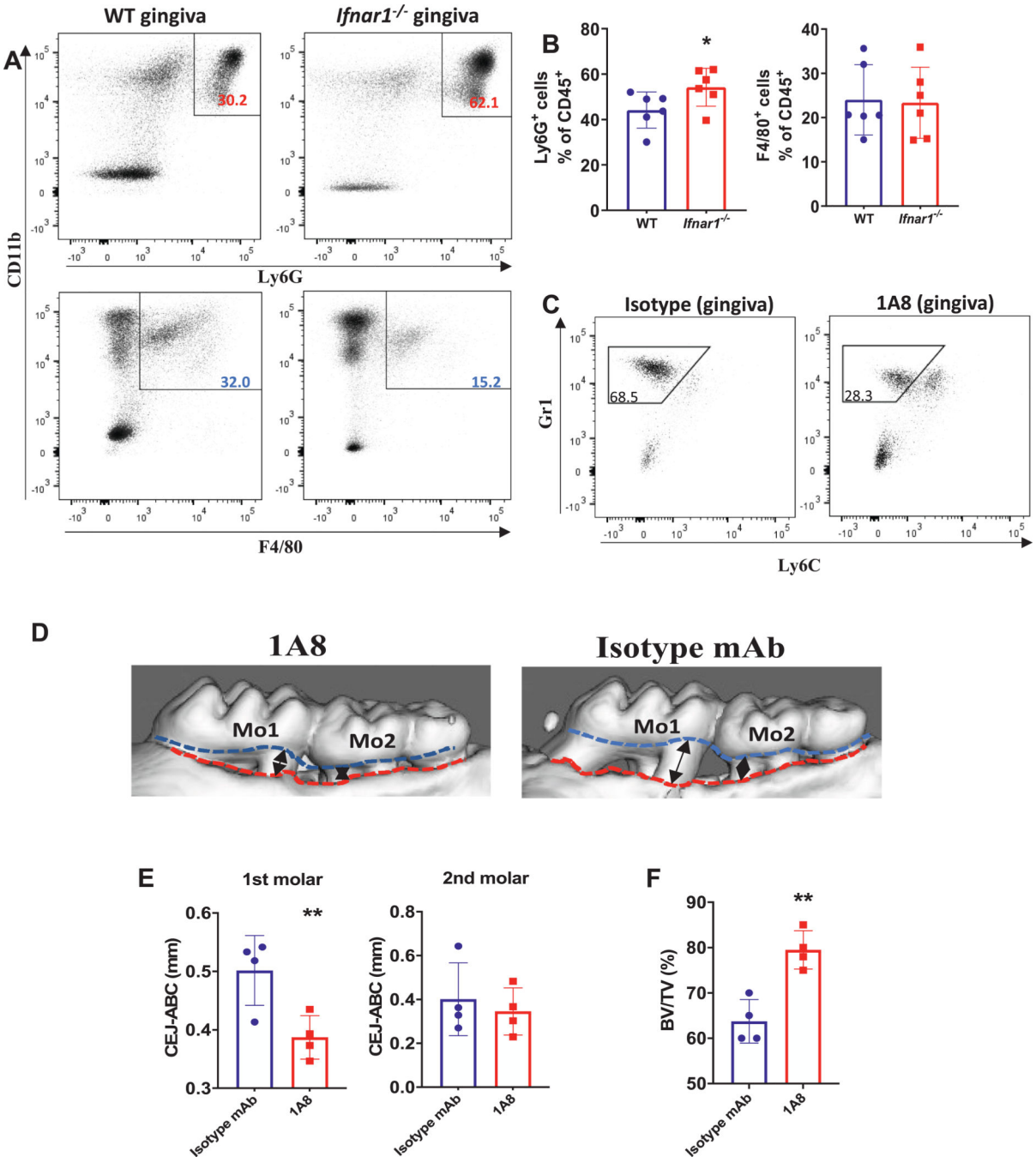

Fig. 4. An integral IFN-I pathway prevents excess neutrophil-mediated severe periodontal bone loss.

Representative flow cytometry plots of the neutrophil population (live $CD45^+CD11b^+Ly6G^+F4/80^-$) and macrophages (live $CD45^+CD11b^+Ly6G^-$ $F4/80^+$) from the ligated gingiva of WT and *Ifnar1*$^{-/-}$ mice on Day 6 post ligature placement are shown (A). The percentage of neutrophils and macrophages out of all live immune cells ($CD45^+$) was compared between the WT group and the *Ifnar1*$^{-/-}$ group (n = 6/group, B). Representative flow cytometry plots show the neutrophil population ($CD45^+CD11b^+Gr1^+Ly6C^{int}$) in gingiva from the isotype control monoclonal antibody

(mAb) IgG2a- or the anti-mouse Ly6G antibody (1A8)-treated mice (C). Representative micro-CT images of the alveolar bone level are shown for *Ifnar1*$^{-/-}$ mice treated with the isotype mAb or 1A8 antibody in the LIP model (D). The linear bone loss (CEJ-ABC) at the distal root of the first molar (Mo1) and the mesial root of the second molar (Mo2) was compared between the isotype IgG2a control- and 1A8-treated mice (n = 4/group, E). The volumetric analysis of bone loss quantified by BV/TV was compared between the IgG2a isotype control antibody- and 1A8-treated mice in the ligated *Ifnar1*$^{-/-}$ mice (F). Quantitative data are presented by mean ± SD. The unpaired t-test was applied for data analysis. * $p < 0.05$; ** $p < 0.01$.

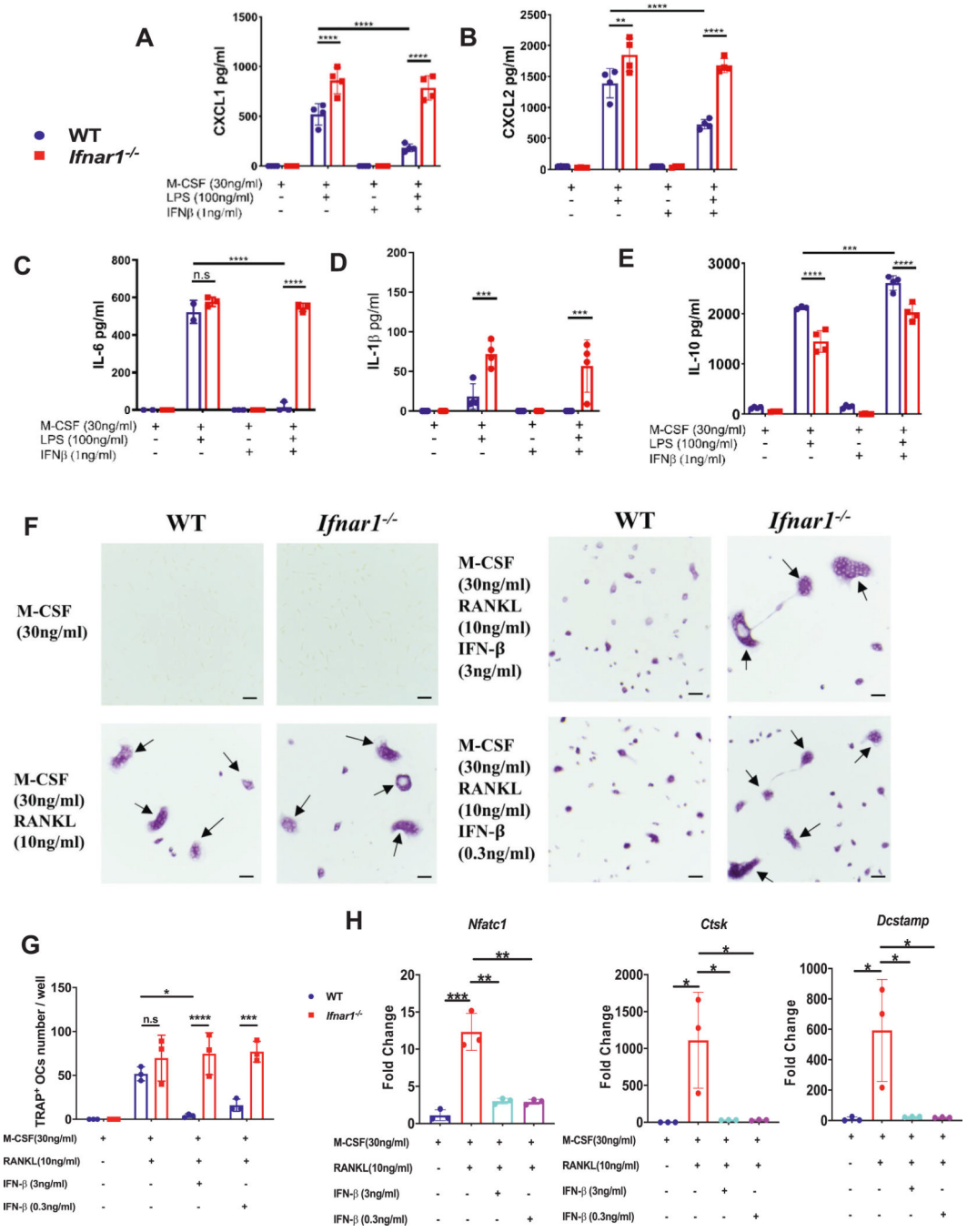

Fig. 5. IFN-β inhibits the LPS-induced inflammatory molecule secretion and the RANKL-mediated osteoclastogenesis in differentiated bone marrow-derived monocytes (BMDMs).

BMDMs were isolated from the WT and *Ifnar1*$^{-/-}$ mice and *ex vivo* differentiated into macrophages in the presence of M-CSF for 3 days. Then, the differentiated macrophages were stimulated with *E. coli* LPS for 18 h with or without the IFN-β cotreatment. The levels of secreted chemokines CXCL1 (A) and CXCL2 (B) and cytokines IL-6 (C) and IL-1β (D) were determined by ELISA and compared between WT and *Ifnar1*$^{-/-}$ cells. The level of anti-inflammatory cytokines IL-10 (E) was also compared. Representative osteoclasts, which are defined by cells with >3 nuclei and positive for TRAP staining, differentiated

from BMDMs, are shown under different treatment conditions (F). Numbers of $TRAP^{+}$ osteoclasts (OCs) were compared between the WT and *Ifnar1*$^{-/-}$ cells (G). The transcription levels of several essential OC-specific genes were compared among differentiated BMDMs under different treatments (H). Quantitative data are presented by mean ± SD for a representative experiment out of at least three independent experiments. Two-way ANOVA was applied to the ELISA data and osteoclast quantification, while one-way ANOVA was used to analyze the transcriptional expression data. *$p < 0.05$. **$p < 0.01$, ***$p < 0.001$, ****$p < 0.0001$, ns, not significant. The scale bars indicate 50 μm.

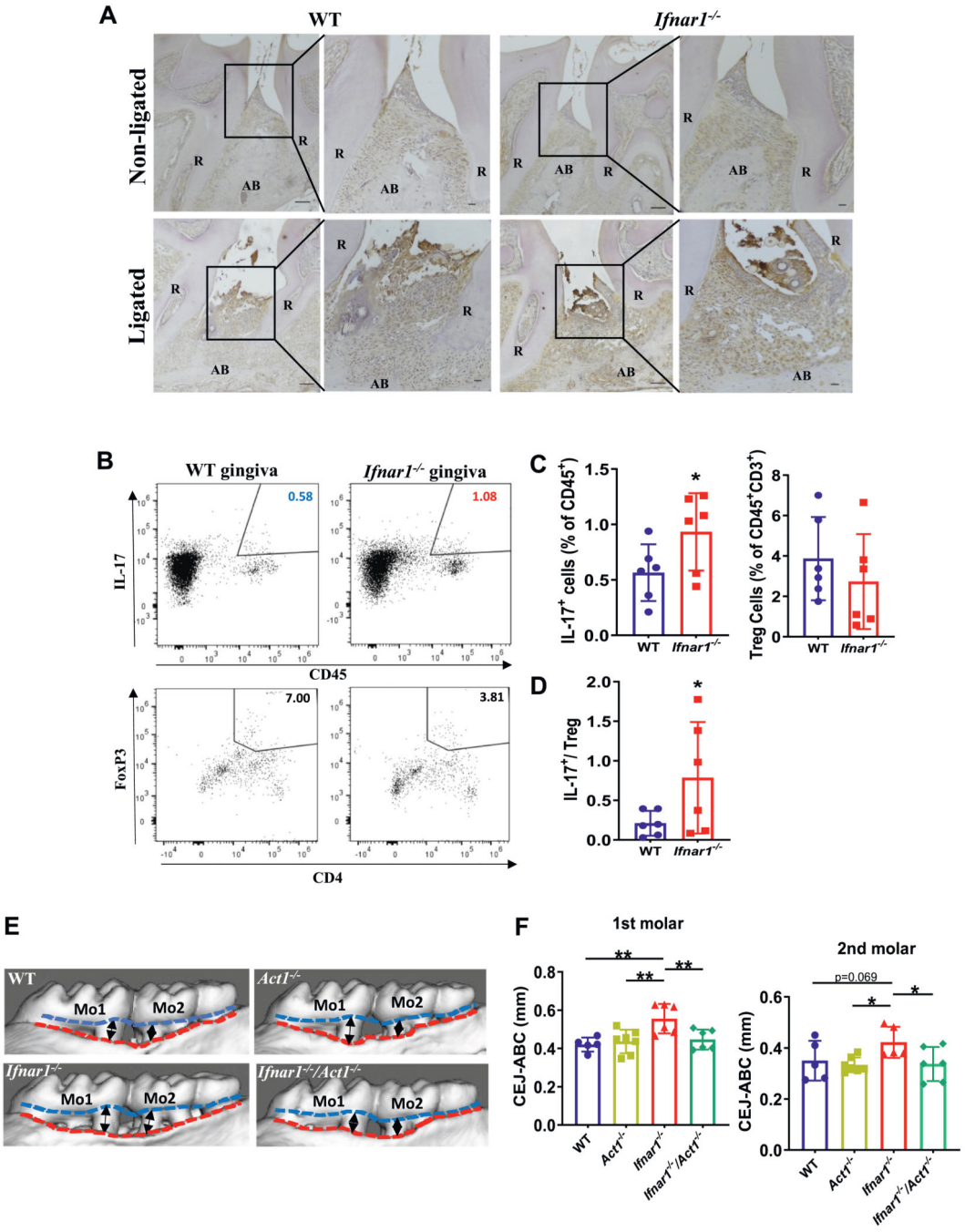

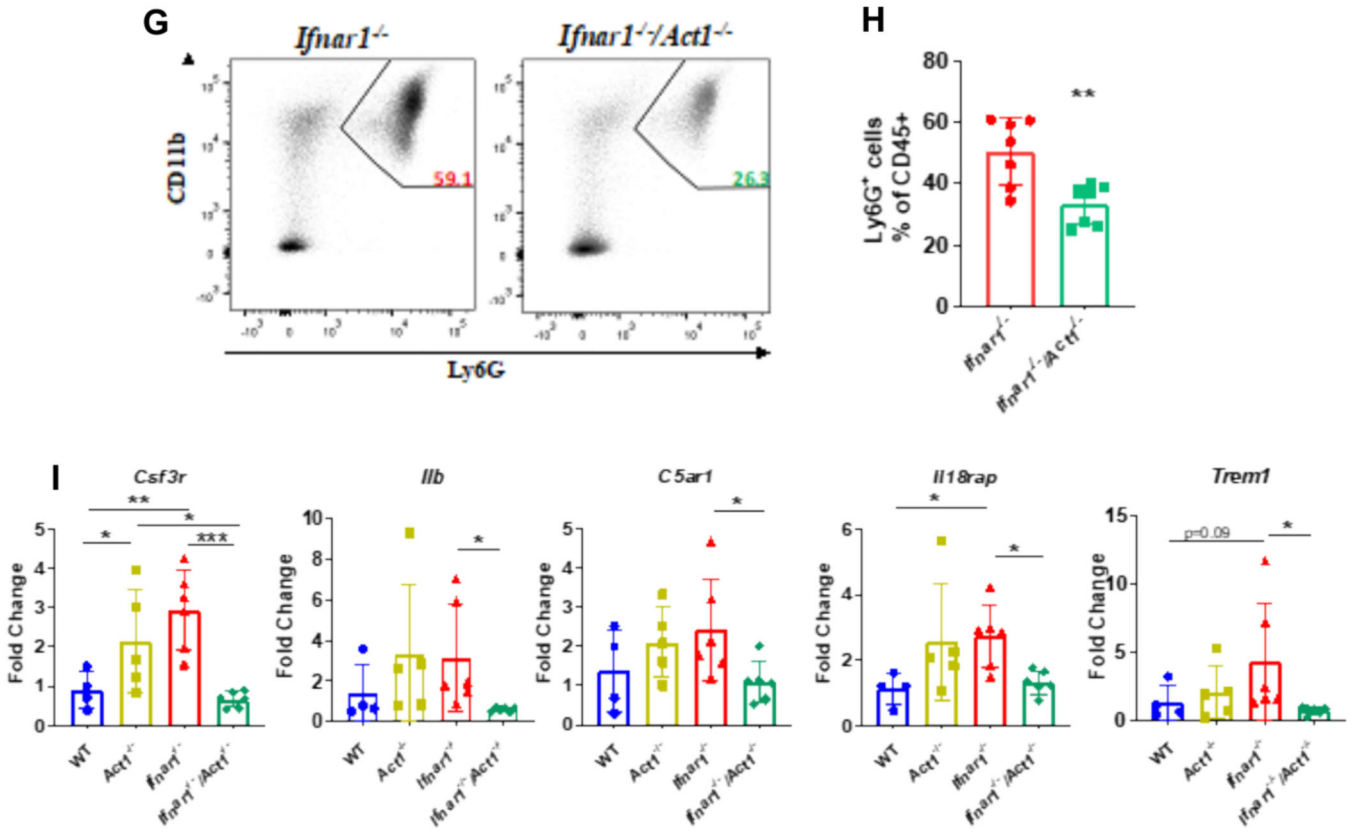

Fig. 6. Overactivation of an IL-17-neutrophil axis in the absence of the IFN-I pathway leads to severe alveolar bone loss in the LIP model.

Representative IHC staining of the IL-17A in the non-ligated and ligated periodontium of the WT and *Ifnar1*$^{-/-}$ mouse maxilla is shown (A). The representative flow cytometry plots of IL-17^{+} cells (live CD45^{+}RORγt^{+} IL-17^{+}) and Treg cells (live CD45^{+}CD3^{+}CD4^{+}FoxP3^{+}) isolated from the WT and *Ifnar1*$^{-/-}$ ligated gingiva tissue are shown (B). IL-17^{+} and Treg cells were compared between WT and *Ifnar1*$^{-/-}$ mice (n = 6/group, C). The ratio of IL-17^{+} to Treg cells was compared between the two groups of samples (D). The representative micro-CT images of the ligated periodontal alveolar bone are shown for each experimental group: double knockout *Ifnar1*$^{-/-}$/*Act1*$^{-/-}$ mice and the littermate controls including WT, *Act1*$^{-/-}$, and *Ifnar1*$^{-/-}$ mice (E). The alveolar bone loss (CEJ-ABC) at the ligated site was compared among different groups of mice (n = 5–7/group, F). The representative flow cytometry plots of neutrophils (live CD45^{+}CD11b^{+}Ly6G^{+}F4/80^{-}) from the *Ifnar1*$^{-/-}$ and double knockout *Ifnar1*$^{-/-}$/*Act1*$^{-/-}$ mouse gingiva are shown (G). The percentage of neutrophils in the double knockout *Ifnar1*$^{-/-}$/*Act1*$^{-/-}$ gingiva was compared with that in the *Ifnar1*$^{-/-}$ tissues (n = 7/group, H). The transcription of inflammatory genes was compared among different groups of mice in the LIP model (n = 4–6/group, I). Quantitative data are presented by mean ± SD. The unpaired *t*-test was applied to two-group comparisons, while one-way *ANOVA* was used to analyze multi-group data. *p < 0.05; **p < 0.01; ***p < 0.001. The scale bars of the left-side images of each panel indicate 100 μm; the scale bars of the right-side images of each panel represent 50 μm. “R” represents root; “AB” indicates alveolar bone.

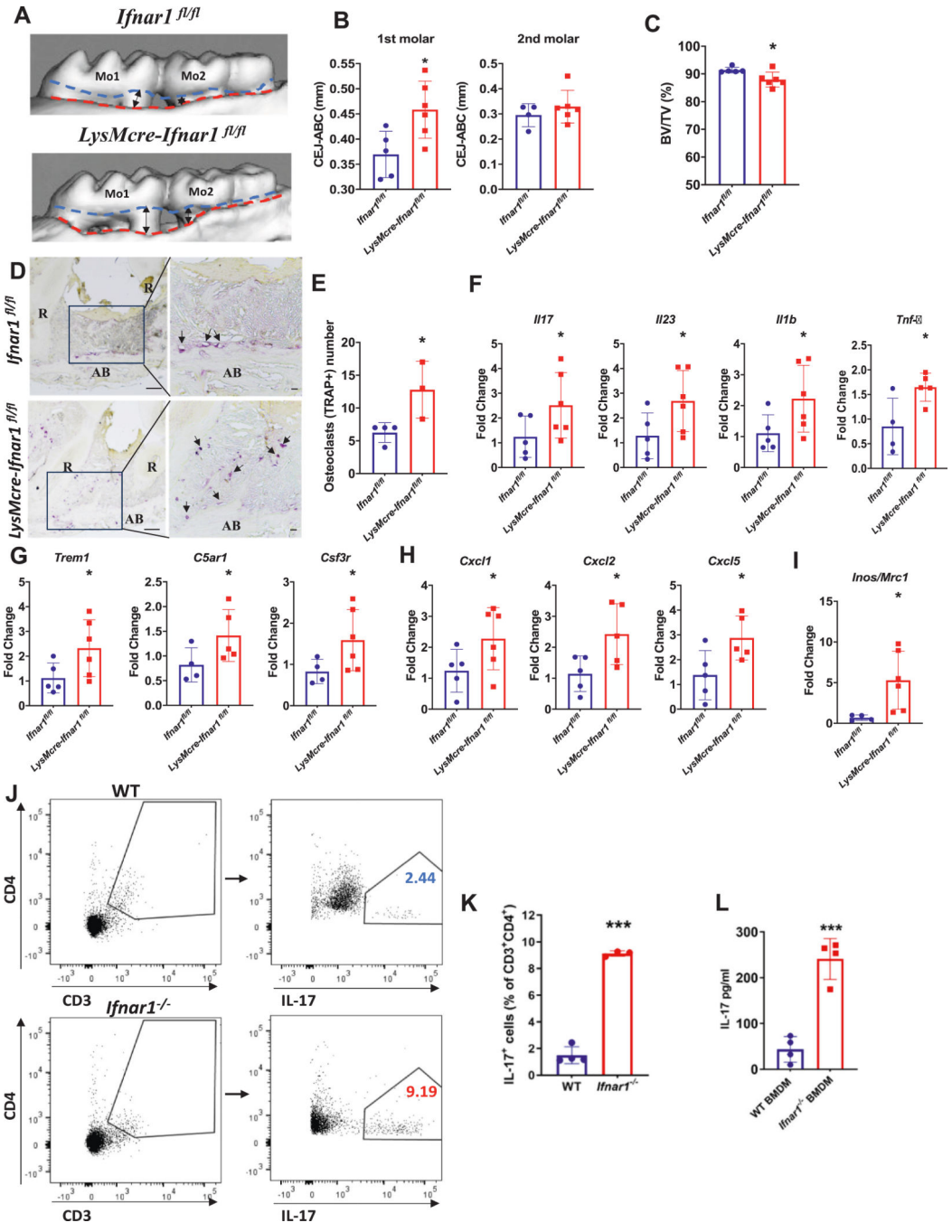

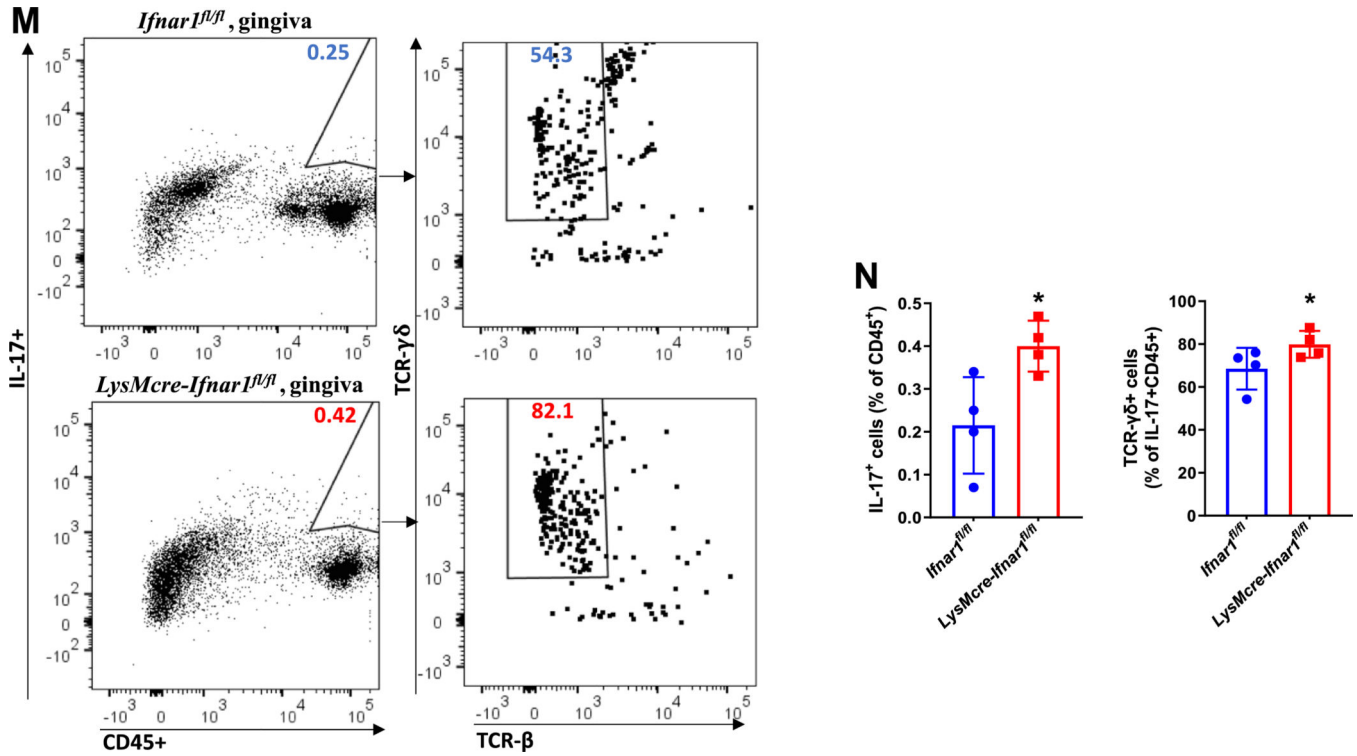

Fig. 7. The IFN-I signaling in myeloid cells prevents severe bone loss by inhibiting the IL-17$^+$ γδ-T cell-mediated inflammatory response.

Representative micro-CT images of the ligated maxillary Mo1 and Mo2 in the *Ifnar1*$^{fl/fl}$ control and the myeloid-specific *Ifnar1* deficient (*LysMcre-Ifnar1*$^{fl/fl}$) mice are shown (A). The alveolar bone resorption (CEJ-ABC) in *LysMcre-Ifnar1*$^{fl/fl}$ mice was compared with the *Ifnar1*$^{fl/fl}$ mice in the LIP model (n = 4–6/group, B). The volumetric analysis of residual bone represented by volume fraction (BV/TV) in the *LysMcre-Ifnar1*$^{fl/fl}$ mice was compared with the control *Ifnar1*$^{fl/fl}$ mice (C). Representative TRAP staining of osteoclasts in the periodontium histology sections is shown (D). Arrows indicate representative TRAP$^+$ osteoclasts. “R” indicates roots; “AB” represents alveolar bone. The osteoclast numbers were compared between the two groups of periodontal tissues (n = 3–4/group, E). The transcriptional level of *Il17*, *Il23*, *Il1b,* and *Tnfa* in the *LysMcre-Ifnar1*$^{fl/fl}$ mouse gingiva was compared to the control *Ifnar1*$^{fl/fl}$ gingival tissue (F). Transcription of genes in innate immunity was compared in the ligated gingival tissue between the two groups of mice (G and H). The ratio of the transcriptional level of *Inos* to *Mrc1* is shown (I). n = 4–6/group for the real-time-qPCR analysis. Representative flow cytometry plots of Th17 populations (live CD45$^+$CD3$^+$CD4$^+$IL-17$^+$) differentiated from the WT naïve CD4$^+$ T cells co-cultured with either WT (J, upper panel) or *Ifnar1*$^{-/-}$ BMDM-derived LPS-stimulated macrophages (J, lower panel). The percentage of Th17 (CD45$^+$CD3$^+$CD4$^+$ IL-17$^+$) cells out of CD4$^+$ T cells co-cultured with the LPS-stimulated *Ifnar1*$^{-/-}$ macrophages was compared to that of the CD4$^+$ T cells co-cultured with the stimulated WT macrophages (K). The supernatant level of IL-17 in the co-culture of the CD4$^+$ T cells with the *Ifnar1*$^{-/-}$ macrophages was compared to that of the co-culture with the WT macrophages (n = 4/group, L). Representative flow cytometry plots of the IL-17$^+$ cells (live CD45$^+$RORγt$^+$IL-17$^+$, left panel) and the IL-17$^+$ γδ T cells (right panel) in the ligated gingiva are shown (M). The percentage of IL-17$^+$ cells

and the IL-17^{+} $_{\gamma\delta}$ T cells in the ligated gingiva of the *LysMcre-Ifnar1*$^{fl/fl}$ mice was compared with the *Ifnar1*$^{fl/fl}$ mice (n = 4/group, N). Quantitative data are presented by mean ± SD. The unpaired *t*-test was applied for statistical analysis. *p < 0.05; ***p < 0.001. The scale bars of the left-side image panel represent 100 μm; the right-side image panel scale bars represent 50 μm.

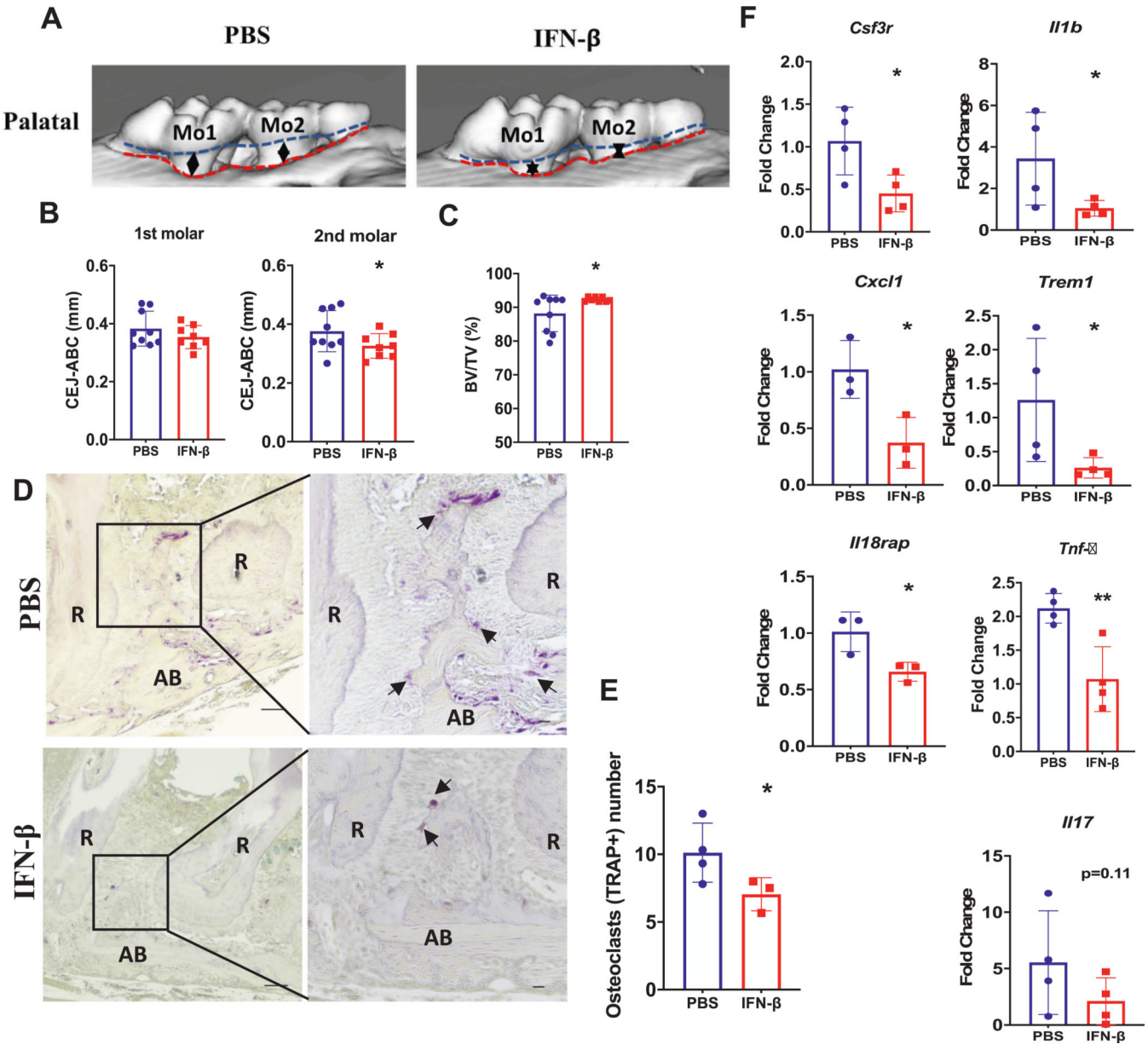

Fig. 8. Locally delivered IFN-β alleviates alveolar bone loss in the LIP model.

Representative micro-CT images (palatal view) of the alveolar periodontal bone at the ligated maxillary Mo1 and Mo2 in WT mice that received PBS or IFN-β treatment are shown (A). The alveolar bone loss at the ligated palatal root of Mo1 and Mo2 was compared between the PBS-treated and the IFN-β-treated mice (n = 8–9/group, B). The volumetric analysis of bone loss represented by volume fraction (BV/TV) was compared between the two groups (C). Representative TRAP staining in the periodontium from the PBS- or the IFN-β-treated mice is shown (D). "R" indicates roots; "AB" represents alveolar bone. The osteoclast numbers were quantified and compared between the PBS-treated and IFN-β treated mice (n = 3–4/group, E). The transcriptional level of inflammatory genes in the ligated gingiva from mice with different treatments was compared (F). Quantitative data are shown as mean ± SD. The unpaired t-test was applied for the statistical analysis. * $p < 0.05$;

**p < 0.01. The scale bars of the left-side image panel represent 100 μm; the right-side image panel scale bars represent 50 μm.